Acta Crystallographica Section B
Structural Science
ISSN 0108-7681

Phosphate tungsten bronze series: crystallographic and structural properties of low-dimensional conductors

P. Roussel,[a] O. Pérez[b]* and Ph. Labbé[b]

[a]Institut für Kristallographie, RWTH Aachen, 52056 Aachen, Germany, and [b]Laboratoire CRISMAT (UMR CNRS 6508), ISMRA, 6 Boulevard du Maréchal Juin, 14050 Caen, France

Correspondence e-mail: olivier.perez@ismra.fr

Received 25 September 2000
Accepted 12 June 2001

Phosphate tungsten bronzes have been shown to be conductors of low dimensionality. A review of the crystallographic and structural properties of this huge series of compounds is given here, corresponding to the present knowledge of the different X-ray studies and electron microscopy investigations. Three main families are described, monophosphate tungsten bronzes, $A_x(PO_2)_4(WO_3)_{2m}$, either with pentagonal tunnels (MPTBp) or with hexagonal tunnels (MPTBh), and diphosphate tungsten bronzes, $A_x(P_2O_4)_2(WO_3)_{2m}$, mainly with hexagonal tunnels (DPTBh). The general aspect of these crystal structures may be described as a building of polyhedra sharing oxygen corners made of regular stacking of WO_3-type slabs with a thickness function of m, joined by slices of tetrahedral PO_4 phosphate or P_2O_7 diphosphate groups. The relations of the different slabs with respect to the basic perovskite structure are mentioned. The structural description is focused on the tilt phenomenon of the WO_6 octahedra inside a slab of WO_3-type. In this respect, a comparison with the different phases of the WO_3 crystal structures is established. The various modes of tilting and the different possible connections between two adjacent WO_3-type slabs involve a great variety of structures with different symmetries, as well as the existence of numerous twins in MPTBp's. Several phase transitions, with the appearance of diffuse scattering and modulation phenomena, were analysed by X-ray scattering measurements and through the temperature dependence of various physical properties for the MPTBp's. The role of the W displacements within the WO_3-type slabs, in two modulated structures (m = 4 and m = 10), already solved, is discussed. Finally, the complexity of the structural aspects of DPTBh's is explained on the basis of the average structures which are the only ones solved.

Philippe Labbé was born in Le Havre, France, in 1939. He was awarded his D.Sc. in physics from the University of Caen in 1978, where he is currently Professor and Head of the Materials Crystallography Laboratory. He will retire from these positions in July 2001. His research interests lie in the areas of X-ray diffraction techniques, and their application to the determination of inorganic and modulated structures and small molecules. He has spent many years studying the structures and properties of the phosphate tungsten bronzes. He has a deep interest in teaching, and many students have gained their doctorates under his supervision, including the two co-authors of this review.

Pascal Roussel was born in Alencon, France, in 1971. He was awarded his Ph.D. from the University of Caen in 1999 for his studies on the phosphate tungsten bronzes. He then worked for 1 year in the Institut für Kristallographie der RWTH Aachen (Germany). He is now a Senior Scientist at CNRS in the LCPS Laboratory of Villeneuve d'Ascq (France) where he is working on structure determination using diffraction techniques.

Olivier Pérez was born in Beauvais, France, in 1971. He obtained his Ph.D. from the University of Caen in 1997 for studies of incommensurate and disordered structures. After a period at the 'Delegation Générale pour l'Armement', he returned to Caen as a Senior Scientist at CNRS. He is currently working on crystal growth and the application of crystallographic techniques.

1. Introduction

The first crystal of phosphate tungsten bronze was synthesized by chance in 1978 and was the only crystal of its kind found in the reaction ampoule. At this time, Raveau and co-workers at the CRISMAT Laboratory, Caen, France, studied the crystal structures of the hexagonal rubidium tungsten bronzes Rb_xWO_3 (Labbé *et al.*, 1978), varying the x ratio of Rb. From different mixtures of composition $Rb_{0.20}WO_3$, prepared in evacuated silica ampoules at 1173 K, three small crystals were selected and tested using the Weissenberg photographic method. One of the crystals tested was evidently different from the others, but time did not permit further study and it was set aside. Approximately 1 year later, the structure of this crystal was undertaken, without knowledge of its composition because at this time no non-destructive analysis was available

in the laboratory. It was first thought that another form of $Rb_{0.20}WO_3$ had been found, but all attempts to synthesize such a crystal from the composition $Rb_{0.20}WO_3$ in a platinum crucible *in vacuo* were unsuccessful. Gradually it was becoming clear that the structure was a combination of WO_6 octahedra and tetrahedral X_2O_7 groups, the X atom being unknown. The reaction of the product with the silicon of the silica tube was immediately considered, but again all attempts to prepare a compound including the observed cell parameters in the system Rb—Si—W—O were also unsuccessful. Michel Goreaud, one of the chemists at the laboratory, suggested that X might be phosphorus, which appeared as an impurity in the silica ampoule, and whose size and atomic number are very close to those of Si. This idea was analysed and confirmed from the detailed study of the Rb—P—W—O system.

A new oxide with the composition $Rb_{0.8}P_4W_{16}O_{56}$ (Giroult *et al.*, 1980) was thus isolated. It was the first 'diphosphate tungsten bronze', the official name given by Kihlborg (1982), a valuable replacement for previous nomenclature which included tungsten pyrophosphates or tungstophosphates. Afterwards, the typical features of the previous compound generated new ideas of structural arrangements, including the remarkable adaptability of PO_4 tetrahedra to a WO_3-type lattice and also their analogy with the molybdenum bronzes. The monophosphate tungsten bronze families were discovered and the crystal structures of different members were solved and refined. In 1988, Arne Magnéli visited the CRISMAT Laboratory and Bernard Raveau showed him a cardboard model of the $P_4W_{12}O_{44}$ structure. He recognized immediately in this collection of octahedra and tetrahedra the counterpart of the structure of γ-Mo_4O_{11} that he had studied and solved 40 years earlier (Magnéli, 1948). He inspected this model for a long time, enjoying substituting Mo for W and P atoms.

It became evident that one could expect, for the phosphate tungsten bronze compounds, physical properties of low dimensionality similar to those encountered in the molybdenum bronze system (Pouget *et al.*, 1983; Schlenker, 1989), including unusual properties such as charge density, wave-driven, metal-to-insulator transitions or insulator-to-superconductor transitions (Greenblatt, 1996). The first study came from Greenblatt and co-workers in a paper entitled 'Electronic instabilities in the quasi-two-dimensional monophosphate tungsten bronze $P_4W_{12}O_{44}$' (Wang, Greenblatt, Rachidi, Canadell, Whangbo & Vadlamannati, 1989*b*).

Later, the transport properties and magnetic characterization of these series of compounds were widely investigated (Greenblatt, 1993; Schlenker, Dumas *et al.*, 1996). Then, band structure calculations (Canadell & Whangbo, 1990) and X-ray diffuse scattering measurements (Foury *et al.*, 1991*a*) led to a new concept called 'hidden nesting', related to the Fermi surface topology (Whangbo *et al.*, 1991). Generally, the electronic anisotropy of a given compound is strongly related to its structural anisotropy. However, it is possible that the electronic anisotropy appears weaker than the structural anisotropy. This is precisely the case for the monophosphate tungsten bronzes in which a 'hidden unidimensionality' was shown (Foury & Pouget, 1993).

From the great variety of physical properties discovered in these series of compounds, and particularly in the monophosphate tungsten bronze families, it seemed that a review limited to their structural properties, as determined from different X-ray studies, numerous electron microscopy investigations and also from the X-ray diffuse scattering observations, would be of interest. Two main families can be distinguished:

(i) The monophosphate tungsten bronzes (MPTB) with the formulation $(PO_2)_4(WO_3)_{2m}$ and $A_x(PO_2)_4(WO_3)_{2m}$, according to the absence or presence of an inserted cation (A) in the tunnels of the structure, where x is the stoichiometry of the small-sized cation (A = Na, K, Pb).

(ii) The diphosphate tungsten bronzes (DPTB), with the general formula $A_x(P_2O_4)_2(WO_3)_{2m}$, where the inserted cation A is of larger size (K, Ba, Rb, Tl and Cs).

In both cases, m is a parameter which takes, *a priori*, all the integer values, except zero. From the electron microscopy observations, m rises to high values, but the X-ray single-crystal resolutions are limited to $m = 14$ in the monophosphate tungsten bronzes and to $m = 10$ in the diphosphate tungsten bronzes.

2. Structural relations between the different tungsten bronzes

2.1. Relations between perovskite and phosphate tungsten bronze structures

Generally speaking, the crystal structures of the different phosphate tungsten bronzes are described as layered structures which are built of regular stacking of slabs with an ReO_3-type structure separated by slices of phosphate (PO_4) or diphosphate (P_2O_7) groups. This elementary description involves slabs, built up of WO_6 octahedra sharing corners in a three-dimensional network, with different orientations from one family to another and with variable thickness from one compound to another of the same family.

The possibility of substituting one or two WO_6 octahedra for one or two PO_4 tetrahedra is illustrated in Fig. 1. Consider a classical perovskite cage made up of eight WO_6 octahedra sharing corners; it is clear that one octahedron may be substituted for a PO_4 tetrahedron or that two adjacent octahedra may be substituted for a P_2O_7 diphosphate group built

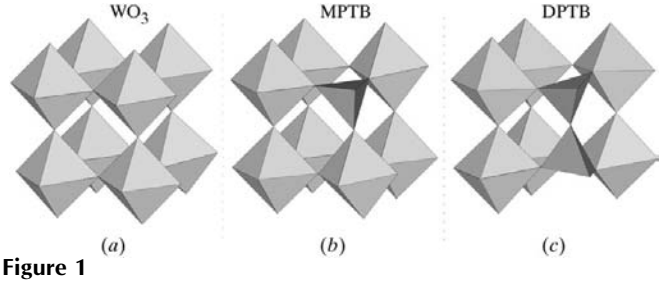

Figure 1
Replacement of WO_6 octahedra in a structure of ReO_3-type: (*a*) classical perovskite cage; (*b*) one WO_6 octahedron is substituted for a PO_4 tetrahedron leading to monophosphate tungsten bronzes (MPTB); (*c*) two adjacent WO_6 octahedra sharing corners are substituted for a P_2O_7 diphosphate group leading to diphosphate tungsten bronzes (DPTB).

of two PO_4 tetrahedra with a common O atom. It is somewhat surprising that such assemblies could be observed, since these substitutions induce slight local deformations because classical O—O distances observed in a PO_4 tetrahedron ($\simeq$ 2.5 Å) are always less than those observed in a WO_6 octahedron ($\simeq$ 2.7 Å). This feature may induce three types of deformation:

(i) a distortion of the neighbouring WO_6 octahedra, *i.e.* a lengthening of some of their O—O distances,

(ii) a possible tilting of these octahedra and

(iii) a possible displacement of the W atoms inside the octahedra involving an off-centred W position and thus different distributions of the six W—O distances.

The only modifications of the O—O distances are caused by a regular distribution of phosphate sets which delimit the edges of the slabs.

Reviewing the papers which describe the different members of these structural families, one notices that the perception of the slabs evolves gradually. In the early papers, the 'WO_3' octahedral slabs are only built with WO_6 octahedra sharing corners and connected through 'slices' of PO_4 tetrahedra. The thickness of one slab is directly related to the length of linear strings of WO_6 octahedra whose directions are precisely those of the reference axes of the perovskite. Two neighbouring strings along $[001]_p$ (Fig. 2) have either the same number of octahedra ($m/2$) for the even m members, or differ by one unit, $[(m+1)/2]$ and $[(m-1)/2]$ for odd m members. This description was then improved, considering the length of the strings along other reference axes $[100]_p$ or $[010]_p$ of the perovskite (shaded rows in Fig. 2): indeed, whatever the m parity, the number of WO_6 octahedra in this direction is the same and equal to m. These strings will be referred to later as 'segments'. The m value is consequently directly related to the thickness of an octahedral slab. As the PO_4 tetrahedra or the P_2O_7 groups are strongly connected to one octahedral slab, leaving only one oxygen per tetrahedron devoted to the connection with an adjacent slab, the tetrahedra are later included in the slab, giving the boundaries on each side and contributing towards the thickness of the slab. The different crystal structures result from the joining of such slabs. In the monophosphates, the lateral PO_4 tetrahedron is strongly connected to three O atoms of three WO_6 octahedra of the slab and leaves free a fourth oxygen apex with which it may be joined to an adjacent slab without extra distortion. In the diphosphates, the lateral P_2O_7 group is strongly connected to four O atoms of four WO_6 octahedra of the slab leaving two free O atoms with which it is possible to join a similar slab.

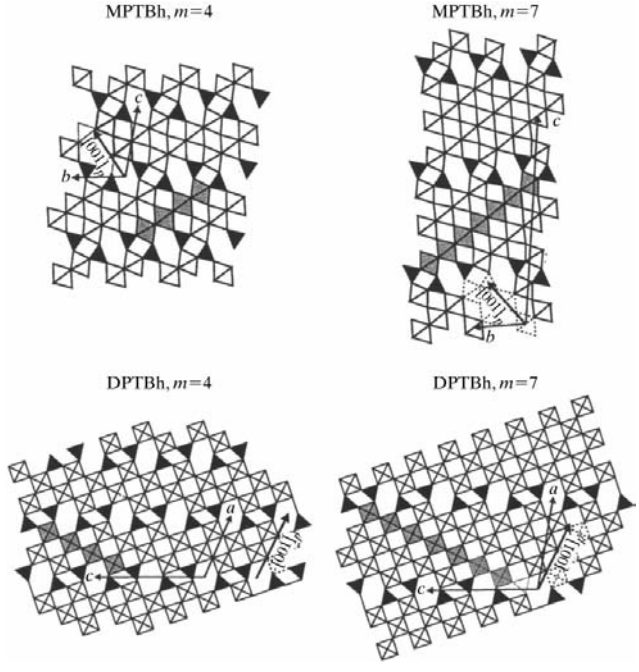

Figure 2
Mono- and diphosphate tungsten bronzes with hexagonal tunnels. In all cases, the thickness of a slab is related to the number m of WO_6 octahedra along the shaded rows.

2.2. Monophosphate tungsten bronzes (MPTB)

The basic element to be considered is a mixed slab of WO_3-type sharing corners with PO_4 tetrahedra. The orientation of the slabs may be defined with respect to the perovskite axes $[100]_p$, $[010]_p$ and $[001]_p$. In the case of the monophosphate tungsten bronzes (MPTB), the slabs are parallel to $(112)_p$ and are usually all of the same thickness in a given compound. Two adjacent slabs may be joined in two different ways (Fig. 3), leading to two different families of monophosphate tungsten bronzes. Firstly, two adjacent slabs, connected by O atoms, are images by 180° rotation; at the interface, cages with pentagonal windows appear and the related family is known as 'MonoPhosphate Tungsten Bronzes with pentagonal tunnels' (MPTBp). Secondly, two adjacent slabs, always connected by O atoms, are only deduced from a translation. At this interface, cages with hexagonal windows are now formed and the related family is known as 'MonoPhosphate Tungsten Bronzes with hexagonal tunnels' (MPTBh). We will see later that the designation 'tunnels' are not suitable in these cases. The above model implies relationships between the perovskite cell

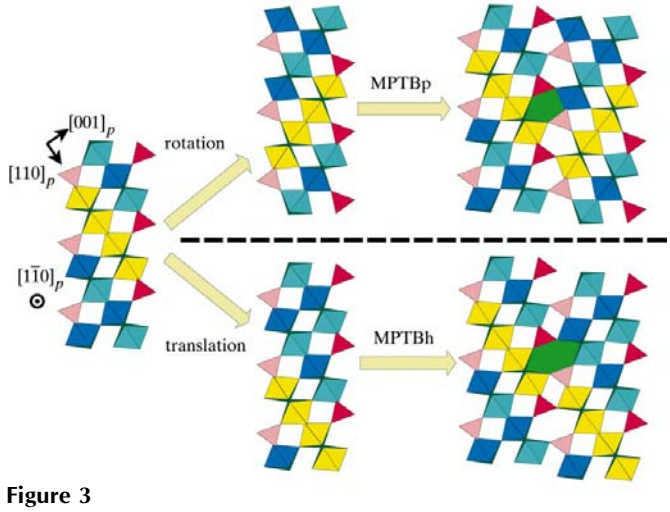

Figure 3
Structural relations between the MPTBp family and the MPTBh family.

(a_p, b_p, c_p) and the MPTB cell, depending on the family and on the thickness of the slabs, *i.e.* the m value.

2.2.1. Monophosphate tungsten bronzes with pentagonal tunnels (MPTBp). The different members of this family correspond to the chemical formula $(PO_2)_4(WO_3)_{2m}$. Except for $P_4W_{10}O_{38}$, the $m = 5$ compound, which also appears as an intergrowth phase, all the slabs always contain the same number of WO_6 octahedra and consequently have the same thickness, corresponding to the following sequence: $(PO_2)(WO_3)_m - (PO_2)(WO_3)_m$. Thus, along the reference axes $[100]_p$ and $[010]_p$ of the perovskite, one observes 'segments' of m octahedra bordered at each end by one tetrahedron (Fig. 3). This results in relations involving the orientations and dimensions of the reference axes (Domengès, Studer & Raveau, 1983)

$$\mathbf{a}_{\mathrm{MPTBp}}//[1\bar{1}0]p,\ \mathbf{b}_{\mathrm{MPTBp}}//[11\bar{1}]p,$$

$$\text{and } \mathbf{c}_{\mathrm{MPTBp}}//[112]p$$

$$\text{with } a_{\mathrm{MPTBp}} \simeq a_p(2)^{1/2},\ b_{\mathrm{MPTBp}} \simeq a_p(3)^{1/2}$$

$$\text{and } c_{\mathrm{MPTBp}} \simeq K + m \times a_p \cos 35^\circ,$$

where K is a constant which takes into account the thickness of the tetrahedra ($K \simeq 2 \times 2.45$ Å) and 35° is approximately the angle between the $\mathbf{c}_{\mathrm{MPTBp}}$ and $[001]_p$ axes.

The cell defined in this way has an orthorhombic symmetry with a and b cell parameters independent of m, and a c parameter which increases linearly with respect to the m value. The previous relations permit easy characterization of a given compound from its parameters and determination of its m value and thus its composition.

Other members of the MPTBp's can be visualized as a regular stacking of slabs of different thickness characterized by m and m' giving the formulation: $(PO_2)(WO_3)_m - (PO_2)(WO_3)_{m'}$. The new periodicity ($d_{001}$) corresponds to the thickness of two successive slabs measured perpendicular to the (**ab**) plane. The cell becomes monoclinic with the following parameters (Roussel, Mather *et al.*, 1998)

$$d_{001} = K + \frac{m + m'}{2} a_p \cos 35^\circ$$

$$\tan \alpha_{\mathrm{MPTBp}} = d_{001} / \frac{m - m'}{2} (a_p \sin 35^\circ)$$

$$c_{\mathrm{MPTBp}} = d_{001} / \sin \alpha_{\mathrm{MPTBp}}$$

$$a_{\mathrm{MPTBp}} = a_p(2)^{1/2},\ b_{\mathrm{MPTBp}} = a_p(3)^{1/2}.$$

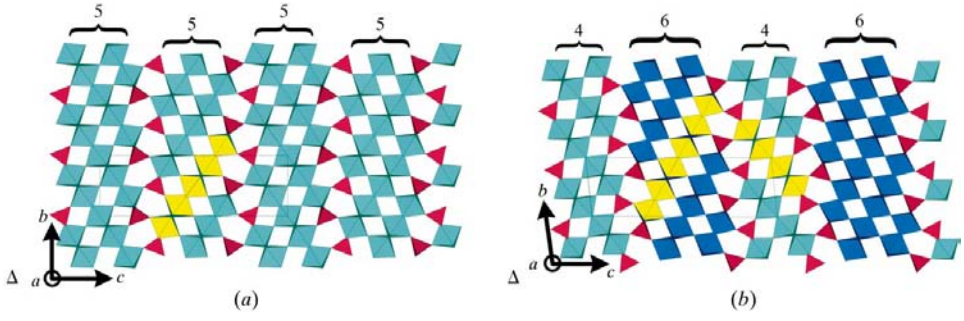

Figure 4
The two forms of $P_4W_{10}O_{38}$ ($m = 5$): (*a*) $m = 5 + 5$; (*b*) $m = 4 + 6$: a regular intergrowth of $m = 4$ and $m = 6$ MPTBp slabs.

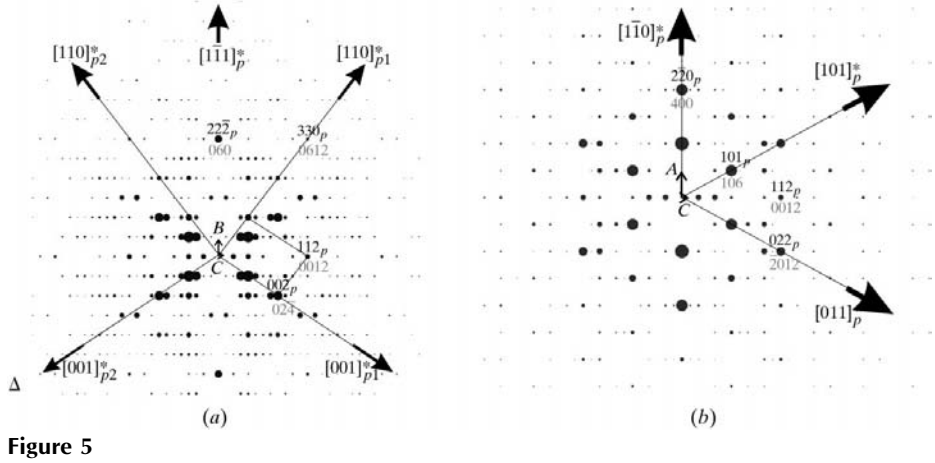

Figure 5
Simulated electron-diffraction pattern with the indexing of stronger maxima both in the perovskite subcell (suffix p) and the $m = 4$ MPTBp cell. (*a*) [100] zone axis. The two perovskite reciprocal spaces, related by the twin symmetry shown Fig. 3, are denoted by the suffixes $p1$ and $p2$. (*b*) [010] zone axis.

However, only the compound $m = 5$ ($P_4W_{10}O_{38}$) appears according to both previous forms, *i.e.* the regular stacking of slabs with five octahedra on the one hand, and the regular intergrowth of slabs with four and six octahedra alternately on the other hand (Fig. 4). All the other members of the family crystallize only with the orthorhombic-type stacking of slabs, all of the same thickness. However, quite irregular intergrowths are often observed by electron diffraction, as in $m = 12$ which involves a monoclinic distortion interpreted as regular alternated stacking of $m = 11$ and $m = 13$ terms (Roussel, Mather *et al.*, 1998). Unfortunately, such samples could not be characterized by HREM and single crystals have never been synthesized.

The intimate relations between the structures in the MPTBp family and the perovskite structure are responsible for particular features in the micrographs obtained by electron diffraction. The patterns show intense spots corresponding to the perovskite

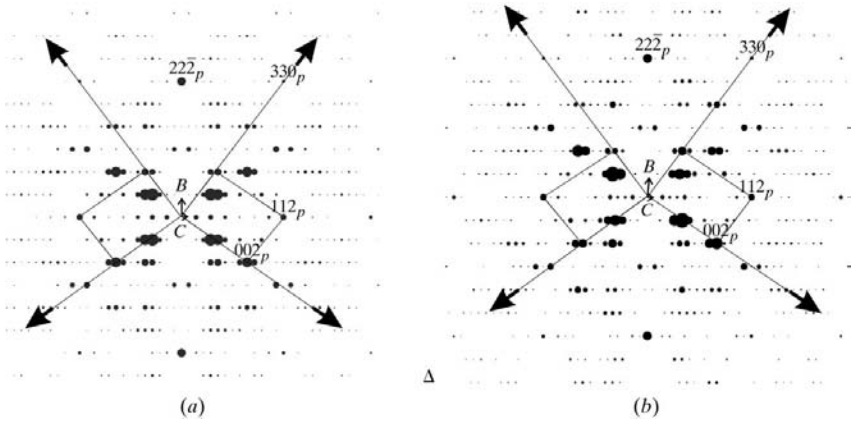

Figure 6
Calculated [100] electron-diffraction patterns of the (*a*) $2m = 5 + 5$ and (*b*) $2m = 4 + 6$ structures. In (*b*) the monoclinic symmetry appears through intensity differences between the contributions of the $m = 4$ and $m = 6$ perovskite subcells.

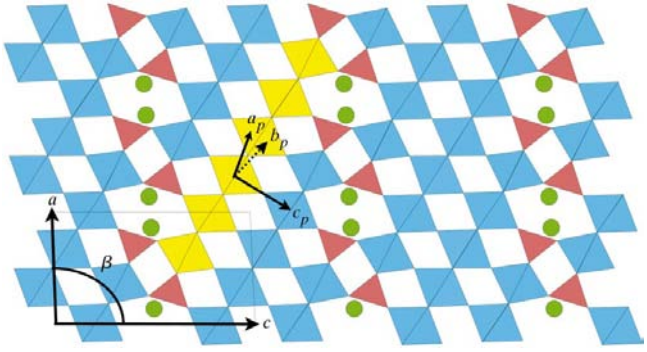

Figure 7
(010) projection of $K_xP_4W_{12}O_{44}$, $m = 6$ term of the family of monophosphate tungsten bronzes with hexagonal tunnels (MPTBh).

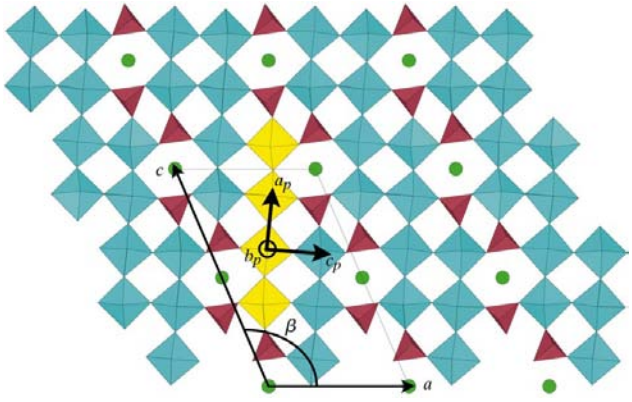

Figure 8
(010) projection of $Rb_xP_4W_8O_{32}$, $m = 4$ term of the family of diphosphate tungsten bronzes with hexagonal tunnels (DPTBh).

subcell which is indexed in the two axial systems. Thus, for $P_4W_8O_{32}$, the $m = 4$ member of the family, the most intense reflection along $\mathbf{c}^*$ is the (00,12), *i.e.* the one with $l = 2(m + 2)$ (Fig. 5). This is not fortuitous and can easily be explained by considering that the thickness of a slab, $c/2$, includes m octahedra and two tetrahedra and is about $(m + 2)d_{112_p}$, and hence the parameter $\mathbf{c}_{\mathrm{MPTBp}} = 2(m + 2)d_{112_p}$. This fact is verified for all the members of the MPTBp series. Moreover, the greater the value of m, the greater the number of octahedra in a slab and consequently the greater the intensity of the reflections in the perovskite subcell (Roussel, Foury *et al.*, 1999).

Considering now the electron micrographs obtained with the two varieties of the $m = 5$ member, the crystal with orthorhombic symmetry (called $2m = 5{+}5$) gives a symmetrical picture with respect to the $\mathbf{b}^*$ axis (Fig. 6*a*), because of the building principle of the series which couples two identical slabs by a rotation about $[11\bar{1}]_p$. On the contrary, the diffraction patterns given by the crystal with monoclinic symmetry (called $2m = 4 + 6$) does not present this symmetrical aspect (Fig. 6*b*), the inequality of the slab thickness inducing differences in the intensity of the spots. Such considerations allow an identification by electron diffraction of the observed phase.

2.2.2. Monophosphate tungsten bronzes with hexagonal tunnels (MPTBh). All members of this series have the same formula: $A_x(PO_2)_4(WO_3)_{2m}$. A is an inserted cation such as Na^+, K^+ or Pb^{2+}, *i.e.* with a ionic radius limited to ∼1.33 Å. The particular building of MPTBh's implies again relations between the reference axes (Domengès *et al.*, 1988). The symmetry is now monoclinic and generally described with β as the monoclinic angle and $\mathbf{c}$ as the longest axis. Consequently, $\mathbf{b}$ is perpendicular to the plane in Fig. 7

$$\mathbf{a}_{\mathrm{MPTBh}}//[11\bar{1}]p,\ \mathbf{b}_{\mathrm{MPTBh}}//[1\bar{1}0]p,$$

$$\text{and } \mathbf{c}_{\mathrm{MPTBh}}//[112]p$$

$$\text{with } a_{\mathrm{MPTBh}} \simeq a_p(3)^{1/2},\ b_{\mathrm{MPTBh}} \simeq a_p(2)^{1/2}$$

$$\text{and } c_{\mathrm{MPTBh}} \times \sin\beta \simeq K/2 + m/2 \times a_p \cos 35^\circ,$$

K always having the same value (2 × 2.45 Å), related to the thickness of a PO_4 slice.

The A cations appear at the level of the tetrahedral slices and they can be visualized through the hexagonal windows visible at the interface of two slabs of WO_3-type (Fig. 7). Depending on the nature of the cation, the c parameter takes, at room temperature, the value calculated above or the doubled value because of slight structural distortions which will be analysed later. Indeed, one observes this c doubling for all members of the series that have been studied with Na^+ or Pb^{2+} as inserted cations.

2.3. Diphosphate tungsten bronzes (DPTB)

The structural building principle of the diphosphate tungsten bronzes is nearly the same as that involved in the

monophosphate tungsten bronzes, but identical slabs of ReO_3-type are now cut parallel to (102) of the perovskite reference axes. These slabs, with a variable thickness according to the length of the segments, are bound on each side by P_2O_7 diphosphate groups and two consecutive slabs are connected through these groups. Two structural types are theoretically possible. If two successive slabs are parallel, hexagonal tunnels appear at the interface; if two consecutive slabs are related by a mirror plane passing through the diphosphate groups, tunnels with a pentagonal section appear at the junction. However, contrary to monophosphate tungsten bronzes, for which the two structure types are frequently encountered, only the diphosphates with hexagonal tunnels are easily synthesized, while those with pentagonal tunnels are only seen in the electron microscope and appearing with numerous defects.

2.3.1. Diphosphate tungsten bronzes with hexagonal tunnels (DPTBh). The members of this family have the general formula $A_x(P_2O_4)_2(WO_3)_{2m}$. They have been isolated for integer m values ($4 \leq m \leq 10$) with different inserted mono- or divalent cations such as K^+, Tl^+, Rb^+ or Ba^{2+}. The regular stacking of identical slabs of ReO_3-type, all of the same width along **a**, involves monoclinic symmetry. As for the MPTBh family, **b** has been chosen along the twofold axis. The cations are situated on the axis of the hexagonal tunnels due to the stacking along **b** of large cages bound by eight WO_6 octahedra and two P_2O_7 groups. The plane of the hexagonal window is perpendicular to the tunnel axis and one can consider here true tunnels. There exist geometrical relations between the DPTBh family cell parameters and those of perovskite (Domengès, Hervieu & Raveau, 1984), as illustrated in Fig. 8 for $m = 4$ ($Rb_xP_4W_8O_{32}$). Thus, for even m values

$$a_{\mathrm{DPTBh}} \simeq K' + (m/2)a_p,\ b_{\mathrm{DPTBh}} = 2a_p$$

$$\text{and } c_{\mathrm{DPTBh}} = a_p(20)^{1/2} \text{ with } K' \simeq 2.6 \text{ Å}$$

$$\text{and } \cos\beta = -5^{1/2}/5 \text{ hence } \beta \simeq 116.6^\circ.$$

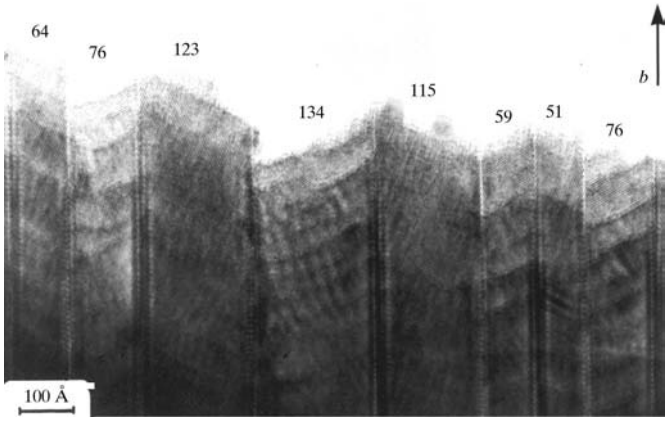

Figure 9
$(P_2O_4)_2(WO_3)_{2m}$ micrographs projected down to (010). High-resolution image showing a random stacking of WO_3 slabs.

We noticed that b, c and β cell parameters are fixed while only a is dependent on m and related to the variable thickness of the slabs: $d_{100} = a\sin\beta$. In fact, the measured β angle is slightly different from 116° ranging from 113.3 to 117.3°, according to local distortions.

In the same manner for odd m values, we have

$$a_{\mathrm{DPTBh}} \simeq K' + a_p\{[1 + [(m-1)^2/4]\}^{1/2},$$

$$b_{\mathrm{DPTBh}} = 2a_p$$

$$\text{and } c_{\mathrm{DPTBh}} = a_p(20)^{1/2} \text{ with } K' \simeq (a_p/2^{1/2}) \simeq 2.6 \text{ Å}$$

$$\text{and } \beta \simeq 116.6^\circ - \omega \text{ with } \omega = \arctan[2/(m+1)].$$

2.3.2. Diphosphate tungsten bronzes with pentagonal tunnels (DPTBp). The members of this fourth family have never been synthesized as pure phases. However, a particular phenomenon has been observed by HREM studies (Hervieu *et al.*, 1985*a*). Some microcrystals exhibit domains of ReO_3-type with various thickness corresponding to large m values (Fig. 9). These domains are symmetrically oriented and are reminiscent of twin domains, with a twin boundary inclined at 65° with respect to the **c** axis of the ReO_3-type structure. This boundary, corresponding to pentagonal tunnels delimited by two P_2O_7 groups and three WO_6 octahedra, suggests an idealized model involving a fourth family of phosphate tungsten bronzes with the formula $(P_2O_4)_2(WO_3)_{2m}$, a new structure type, diphosphate tungsten bronzes with pentagonal tunnels (DPTBp), as illustrated in Fig. 10. The different members of this new family would be characterized by an orthorhombic cell with the following parameters (Hervieu *et al.*, 1985*a*)

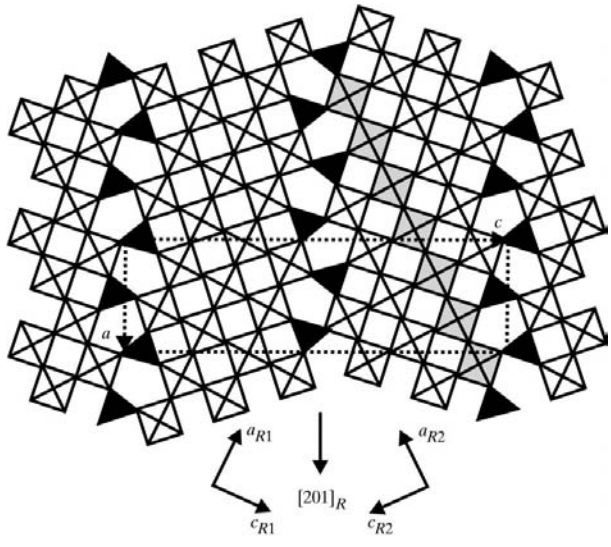

Figure 10
Idealized projection onto (010) of the $m = 7$ member of the $(P_2O_4)_2(WO_3)_{2m}$ structure type. The twin boundary consists of empty pentagonal tunnels.

$$a_{\mathrm{DPTBp}} \simeq a_p(5)^{1/2},\ b_{\mathrm{DPTBp}} \simeq 2a_p$$

$$c_{\mathrm{DPTBp}} \simeq 2m[a_p/(5)^{1/2}] + 2K' \text{ with } K' \simeq 2.6 \text{ Å}.$$

However, from the HREM observations it appeared that no regular member corresponding to this series could be synthesized. Only semi-regular sequences were observed which involve such structural arrangements. The boundary spacing varies in a large domain, but in some crystals a quasi-regular sequence is observed. The junction model was verified by calculated images which confirmed the existence of slices of pentagonal tunnels separating slabs of ReO_3-type. These pentagonal tunnels are supposed to be empty.

2.4. Relationships between MPTB and DPTB crystal structures

The previous descriptions of the polyhedral arrangements in the MPTB and DPTB families of crystal structures are simplified versions of a synthetic building principle. Rouxel (1983) makes a comparison with the buildings in the French 'Henri IV'[1] style, which are constructed by an alternate stacking of bricks and stones slices (Fig. 11), and which allows an understanding of the geometrical intergrowth realised in the four families.

A schematic representation of the existing relationships between the different phosphate tungsten bronze families is given in Fig. 12. The two MPTB families are built up of identical slabs, made of a (112) oriented WO_3-type matrix, and phosphate groups, the connections between the successive slabs being ensured by O atoms common to PO_4 tetrahedra of one layer and to WO_6 octahedra of the adjacent layer. The MPTBh structure is easily deduced from the MPTBp's by a rotation of π of every other slab about an axis perpendicular to the slab plane. This structural relationship is similar to that observed for the DPTB families which exhibit slabs of WO_3-type, oriented (102) with respect to the perovskite axes, and bordered with P_2O_7 groups which join two successive slabs. A π rotation of alternate slabs about an axis perpendicular to the slab plane gives the correspondence between the two structural types.

2.5. Phase diagrams

The stability domain of the phosphate tungsten bronzes with the general formula $K_xNa_y(PO_2)_4(WO_3)_{2m}$ being able to appear in the system K—Na—P—W—O has been established systematically for two particular m values: $m = 4$ and $m = 6$ (Roussel, Groult *et al.* 1999). In that study, the maximal rate of occupation of the host sites for the different cations, Na^+ and K^+, has been considered to be four atoms per chemical formula, *i.e.* $(x + y)_{\max} = 4$. According to this hypothesis, all the tunnel sites are occupied, and consequently all the perovskite cages are empty. From a steric point of view, the insertion of Na^+ in these cages may be realised, since it is observed, for example, in Na_xWO_3 (Wohler, 1825). However, the previous structural determinations of the PTB members with sodium as inserted cations have never shown any electronic residue in the perovskite cages and consequently authors suppose that only the widest sites are occupied. Note, however, that a small quantity of Na statistically distributed in the different perovskite cages should be undetected with X-ray scattering because of the presence of heavy W atoms.

Phase diagrams were constructed from observations made on 150 different syntheses obtained by solid-state reaction, which correspond to different ratios of inserted Na^+ and K^+ cations (different x and y compositions). Samples were prepared from mixtures of $(NH_4)_2HPO_4$, WO_3, W and alkali metal carbonates using a two-step procedure. First, adequate mixtures of $(NH_4)_2HPO_4$, alkali metal carbonate and WO_3 were heated in a platinum crucible at 873 K for 24 h to decompose ammonium phosphate and carbonate. Then, appropriate amounts of metallic tungsten, used as a reducing agent, were added before the mixtures were fired in silica tubes at 1223 K for 48 h. The resulting powder samples were

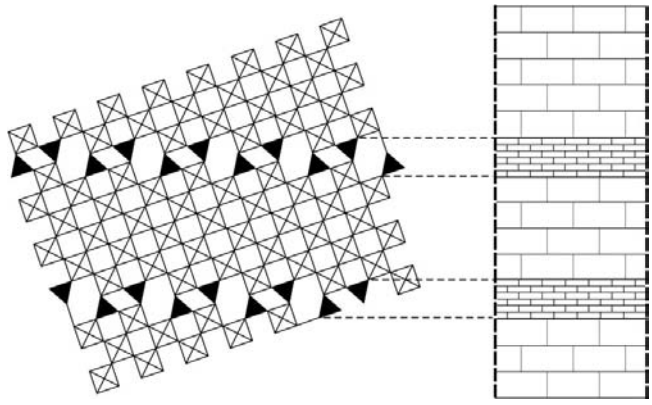

Figure 11
Henri IV building style, where brick and stone layers are alternated, and skeleton of the $m = 8$ member of the DPTBh's.

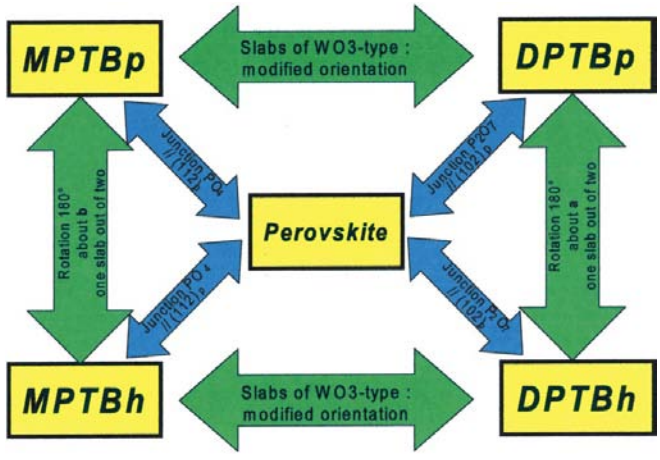

Figure 12
Schematic representation of the existing relations between the various families of phosphate tungsten bronzes.

[1] King of France, 1589–1610.

characterized by X-ray diffraction analysis using a powder diffractometer equipped with a monochromator delivering Cu $K\alpha$ radiation. Single crystals were grown by chemical vapour transport. Typically, a charge of 2 g of powder was heated in a sealed quartz tube placed in a two-zone furnace, the hot zone at 1473 K and the cold zone at 1273 K, separated by a distance of 20 cm. The composition of the crystals was examined by electron probe microanalysis using energy-dispersive spectrometry (EDS).

The results are summarized in phase diagrams [Figs. 13 (m = 4) and 14 (m = 6)]. Thus, in the case of $K_xNa_yP_4W_8O_{32}$ (m = 4), only one single-phase domain corresponding to the MPTBh type is observed, showing that for this member the (MPTBh) type of structure is the most stable. For $2 < (x + y) \leq 4$, the powder diagrams show a mixture of phases, implying other terms than m = 4, as well as 'traditional' bronzes A_xWO_3. A small domain of stability of the MPTBp family, near to $P_4W_8O_{32}$ (x+y = 0), can exist but with a very low alkali metal solubility ($x + y$ = 0.1).

As for $K_xNa_yP_4W_8O_{32}$ (m = 4), a single-phase domain of the MPTBh family is observed for $K_xNa_yP_4W_{12}O_{44}$ (m = 6, Fig. 14), but with a rate of Na^+ and K^+ which can reach $x + y$ = 3, higher than in the case of m = 4 ($x + y$ = 2). However, the main difference between the ternary diagrams m = 6 and m = 4 is the appearance of two additional domains of stability relating respectively to phases of the MPTBp and DPTBh type. This aspect of the phase diagram was innovative because it showed for the first time that sodium can be inserted in the O_{18} cages of the MPTBp structure with an insertion rate $y = 1$. In addition, for $0.75 \leq x \leq 1.2$, compounds $K_xP_4W_{12}O_{44}$ with the DPTBh-type structure were isolated, whereas they are not observed for the m = 4 term. It should be noted that the insertion of Na^+ in the hexagonal tunnels of DPTBh remains limited to very small concentrations, *i.e.* less than 10%. The fact that these two domains of stability are not observed for m = 4 remains unexplained, taking into account the similarity of the networks of m = 4 and m = 6 for the MPTBp structure as well as for the DPTBh structure.

3. Monophosphate tungsten bronze family

3.1. Monophosphates without inserted cation $(PO_2)_4(WO_3)_{2m}$

3.1.1. Symmetry of the family members. The family of monophosphate tungsten bronzes with pentagonal tunnels (MPTBp) was the most studied, both for their physical properties and also for their structural peculiarities. Table 1 summarizes the present knowledge of the 15 members of this family analysed so far. For easier comparison, the cell parameters have been standardized: a, close to 5.30 Å, corresponds to the height of two WO_6 octahedra lying on an edge and is the lattice translation normal to the projection plane in Fig. 3; b, close to 6.55 Å, is the lattice vertical translation which joins, for example, two equivalent PO_4 tetrahedra in the same joining plane. These two parameters are always the same throughout all members of the series. On the other hand, the horizontal cell translation c depends on the m value, therefore, on the thickness of the WO_3-type slabs.

The symmetry suggested by the stacking effect of similar slabs should be identical for all the members as well as their space group. Surprisingly, a large variety of symmetries is observed: two different orthorhombic symmetries ($P2_1cn$ and $P2_12_12_1$), monoclinic with either **b** or **c** as the twofold axis, or triclinic (m = 9; Roussel, Labbé & Groult, 2000). For the most part the structures are acentric, but in three cases a centre of symmetry is detected. Sometimes, the same m value leads to two different models at room temperature. This is the case for $P_4W_{10}O_{38}$ (m = 5), for which two monoclinic structures are observed with two distinct regular stacking modes (Benmoussa *et al.*, 1982; Roussel, Drouard *et al.*, 1999). One of the main features is the very frequent existence of twins in numerous crystals studied in this series. It is obvious that this amazing diversity has its origin in small distortions in the atomic architecture, in other words in the polyhedral arrangement with respect to the ideal structural type. Note that the HREM images are unable to detect such details. However, they have perfectly confirmed the atomic arrangement, revealed the stacking faults and suggested other types of

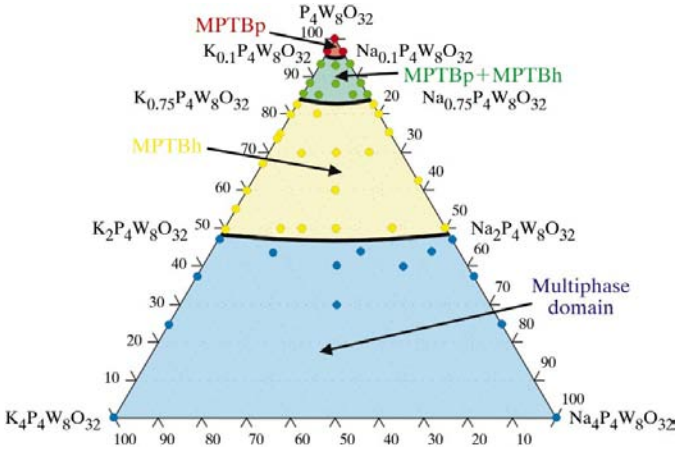

Figure 13
Stability phase domains of phosphate tungsten bronzes $(K_xNa_y)P_4W_8O_{32}$ (m = 4). The thick lines are visual guides.

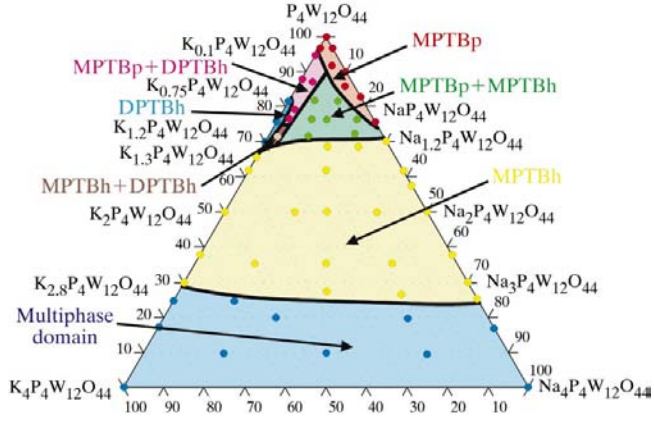

Figure 14
Stability phase domains of phosphate tungsten bronzes $(K_xNa_y)P_4W_{12}O_{44}$ (m = 6). The thick lines are visual guides.

Table 1
The MPTBp series (HT refers to high-temperature phase).

m	Formula	Symmetry and space group	Cell parameters (Å, °)	T_c (K)	Modulation vector $\mathbf{q}^*$	References
2	$P_4W_4O_{20}$	Monoclinic ?	a = 5.22 b = 6.54 c = 11.17 α = 90.34			(*a*), (*b*)
2	$P_4W_4O_{20}$	Orthorhombic $P2_1cn$	a = 5.23 b = 6.55 c = 11.17			(*c*)
4	$P_4W_8O_{32}$	Orthorhombic $P2_12_12_1$	a = 5.28 b = 6.57 c = 17.35	80(±1) 52(±1)	(0.330,0.295,0) (0.340,0,0)	(*d*), (*e*), (*f*), (*g*) (*h*), (*i*), (*j*), (*k*) (*l*), (*m*), (*n*), (*o*) (*p*), (*q*), (*r*), (*s*)
5	$P_4W_{10}O_{38}$	Monoclinic $P2_1/n$	a = 5.28 b = 6.57 c = 20.45 β = 90.40	80(±3) 58(±2)	(0.32,0.29,0) (0.36,0,0)	(*t*), (*u*), (*v*) (*w*)
4 + 6	$P_4W_{10}O_{38}$	Monoclinic $P2_1$	a = 5.28 b = 6.57 c = 20.57 α = 96.18	158(±2) ?	(0.330,0.330,0) (0.33,0,0)	(*p*), (*x*), (*m*), (*y*) (*u*), (*v*), (*w*)
6	$P_4W_{12}O_{44}$	Orthorhombic $P2_12_12_1$	a = 5.29 b = 6.57 c = 23.55	120(±1) 62(±1) ≃ 30	(0.385,0,0) (0.310,0.295,0) (0.29,0.11,0)	(*z*), (*aa*), (*d*), (*e*) (*f*), (*h*), (*o*), (*p*) (*bb*), (*m*), (*cc*), (*dd*) (*ee*), (*j*), (*k*), (*l*)
7	$P_4W_{14}O_{50}$	Monoclinic $P2_1$	a = 5.29 b = 6.56 c = 26.65 β = 90.19	188(±1) 60(±1)	(0.260,0.073,0.27) (0.12,0.03,0.15)	(*d*), (*e*), (*f*), (*p*) (*ff*), (*gg*), (*hh*), (*m*) (*ee*), (*j*), (*k*), (*l*) (*ii*), (*jj*), (*hh*)
8	$P_4W_{16}O_{56}$	Orthorhombic $P2_12_12_1$	a = 5.29 b = 6.55 c = 29.7	≃220 ≃200	(0.47,0.02,0.15) (0.19,0.03,0.15)	(*p*), (*bb*), (*kk*), (*hh*) (*m*), (*cc*), (*ll*), (*mm*) (*w*)
9	$P_4W_{18}O_{62}$	Triclinic $P\bar{1}$	a = 5.28 b = 6.57 c = 32.79 α = 90 β = 90.2 γ = 89.78	565(±5) 330(±5)	(0.5,0,0) (0.17,0,0)	(*m*), (*nn*) (*p*), (*kk*), (*bb*), (*hh*) (*l*), (*ll*), (*mm*) (*w*)
10	$P_4W_{20}O_{68}$	Monoclinic $P2_1(\alpha\ 0\ 0)$	a = 5.30 b = 6.55 c = 35.82 γ = 90.6	≃ 450	(0.43,0,0)	(*n*), (*bb*), (*l*), (*ll*) (*mm*), (*oo*)
11	$P_4W_{22}O_{74}$	Monoclinic ?		560(±5) ?	(0.43,0,0)	(*m*), (*l*), (*mm*)
12 (HT)	$P_4W_{24}O_{80}$	Orthorhombic $P2_12_12_1$	a = 5.31 b = 6.55 c = 42.11			(*m*), (*pp*)
12	$P_4W_{24}O_{80}$	Monoclinic ?	a = 5.31 b = 6.55 c = 42.11 γ = 90.72	535(±5) 500(±5)	(0.12,0,0) (0.50,0,0.5)	(*n*), (*p*), (*bb*), (*kk*) (*qq*), (*rr*), (*mm*), (*pp*)
13	$P_4W_{26}O_{86}$	Monoclinic ?	a = 5.32 b = 6.55 c = 45.04 γ = 91.06	550(±5) 510(±5) 160(±10)	(0.053,0.016,0) (0.5,0,0) (0.178,0.145,0)	(*p*)(*kk*)(*ss*)(*mm*)
14	$P_4W_{28}O_{92}$	Monoclinic $P2_1/n(1/2\ 0\ \gamma)$	a = 5.32 b = 6.54 c = 48.00 γ = 91.04	730/695	(0.5,0,0.5)	(*p*), (*kk*), (*m*), (*mm*)

References: (*a*) Teweldemedhin *et al.* (1991); (*b*) Kinomura *et al.* (1988); (*c*) Wang, Wang & Lii (1989); (*d*) Lehmann *et al.* (1993); (*e*) Rötger *et al.* (1993); (*f*) Rötger *et al.* (1994); (*g*) Teweldemedhin *et al.* (1992); (*h*) Le Touze *et al.* (1995); (*i*) Giroult *et al.* (1981*b*); (*j*) Foury & Pouget (1993); (*k*) Foury, Pouget, Teweldemedhin, Wang & Greenblatt (1993); (*l*) Foury, Pouget, Teweldemedhin, Wang, Greenblatt & Groult (1993); (*m*) Domengès, Hervieu, Raveau & Tilley (1984); (*n*) Schlenker *et al.* (1995); (*o*) Hess *et al.* (1996); (*p*) Schlenker, Hess *et al.* (1996); (*q*) Ludecke *et al.* (2000); (*r*) Ludecke *et al.* (2001); (*s*) Sandre *et al.* (2001); (*t*) Beierlein *et al.* (1999); (*u*) Roussel, Foury *et al.* (1999); (*v*) Foury *et al.* (1999); (*w*) Dumas *et al.* (1999); (*x*) Hess, Le Touze, Schlenker, Dumas & Groult (1997); (*y*) Benmoussa *et al.* (1982); (*z*) Wang, Greenblatt, Rachidi, Canadell & Whangbo (1989*b*); (*aa*) Wang, Greenblatt, Rachidi, Canadell, Whangbo & Vadlamannati, 1989*b*); (*bb*) Witkowski *et al.* (1997); (*cc*) Labbé *et al.* (1986); (*dd*) Foury *et al.* (1991*a*); (*ee*) Foury *et al.* (1991*b*); (*ff*) Hess, Schlenker, Bonfait, Ohm *et al.* (1997); (*gg*) Hess, Schlenker, Bonfait, Marcus *et al.* (1997); (*hh*) Dumas *et al.* (2000); (*ii*) Roussel *et al.* (1996); (*jj*) Domengès *et al.* (1996); (*kk*) Hess, Le Touze, Schlenker, Dumas, Groult & Marcus (1997); (*ll*) Ottolenghi *et al.* (1995); (*mm*) Ottolenghi & Pouget (1996); (*nn*) Roussel, Labbé & Groult (2000); (*oo*) Roussel, Labbé, Leligny *et al.* (2000); (*pp*) Roussel, Mather *et al.* (1998); (*qq*) Yan *et al.* (1995); (*rr*) Yan *et al.* (1994); (*ss*) Hess, Schlenker, Hodeau *et al.* (1997).

connections. Only the structure determinations based on single-crystal X-ray diffraction allowed observations of slight deformations in the atomic arrangements and a precise definition of the nature of the differences between the family members. These differences are due to the tilting of the WO_6 octahedra into the slabs and by the linking process of the successive slabs. At room temperature, for the largest m values satellite reflections are observed involving the existence of a modulation phenomenon. The modulated structure of $P_4W_{20}O_{68}$ (m = 10) has been refined (Roussel, Labbé, Leligny *et al.*, 2000). For the small m values analogous phenomena appear only at low temperature and the modulated structure of $P_4W_8O_{32}$ (m = 4; Ludecke *et al.*, 2000) has been solved at 20 K with the aid of synchrotron radiation. Attempts to solve structures, and particularly to determine O-atom positions, using neutron diffraction on single crystals, failed because neutron-quality crystals could not be synthesized. However, some experiments on $P_4W_{12}O_{44}$ (m = 6) are planned at the Institute Laue–Langevin (ILL Grenoble) using neutrons and powder samples at different temperatures (Pérez *et al.*, 2000).

3.1.2. Tilting mode for all the family members. In a given slab, the shortest segment along $\mathbf{c}_p$, one of the reference axes of perovskite, includes m/2 WO_6 octahedra for even m and (m + 1)/2 or (m − 1)/2 octahedra for odd m. All octahedra of the same segment are tilted by ∼8° in the same direction and therefore in the opposite direction for the four adjacent segments sharing O atoms in the same slab. This early observation (Giroult *et al.*, 1981*a*) is general for all the members of the family. On the other hand,

no tilting is observed in the other two segment directions, whatever the m parity, each consisting of m octahedra. According to Glazer's (1972) notation, the tilt system in all the MPTBp series is ($a^0b^0c^+$), reducing the in-phase tilting along $\mathbf{c}_p$, whereas no tilting is observed along the other two axes $\mathbf{a}_p$ and $\mathbf{b}_p$ (Fig. 15) (Roussel, Labbé & Groult, 2000). This typical feature should be compared to those found in the different phases of WO_3, now precisely known. It has been suggested (Ottolenghi *et al.*, 1995) that when m becomes large, *i.e.* when the thickness of the octahedral slabs becomes sizeable, the structure of the slabs tends to that of WO_3 (Labbé, 1992). However, the tilting systems are quite different, in spite of approximately the same tilt angle (8°). The symbolic notations are the following: For the α variety of WO_3 (Kehl *et al.*, 1952; Vogt *et al.*, 1999), the tetragonal phase ($T > 1010$ K): ($a^0b^0c^-$), indicating an out-of-phase tilt mode in the **c** direction; for the β variety (Salje, 1977; Vogt *et al.*, 1999), the orthorhombic phase ($600 < T < 1010$ K): ($a^0b^+c^-$); for the γ variety (Loopstra & Boldrini, 1966; Loopstra & Rietveld, 1965; Woodward *et al.*, 1997) a monoclinic phase between 290 and 600 K: ($a^-b^+c^-$); and finally, for the two varieties at low temperatures, the triclinic phase δ (Diehl *et al.*, 1978; Woodward *et al.*, 1995) and the second monoclinic phase ε (Woodward *et al.*, 1997): ($a^-b^-c^-$) (Fig. 16). Thus, concerning the octahedral tilting mode, no phase of WO_3 is merged with the octahedral slab structure in the MPTBp family. This observation suggests that the PO_4 tetrahedra in these structures play an essential part towards the tilting mode of the WO_6 octahedra. There is, however, an additional effect. For a given segment along $\mathbf{c}_p$ the rotation may be clockwise or counterclockwise, leading to two possibilities for a given octahedral slab. However, for these two possibilities the positions of the O atoms, which are common to two adjacent slabs, are unchanged, thus offering a greater diversity of connections. From a structural point of view, one needs to distinguish between even m and odd m. This choice is induced by the fact that the even m values have an orthorhombic lattice, whereas the odd m values lead to a monoclinic lattice, but pseudo-orthorhombic with the systematic existence of an observable twin.

3.1.3. Members with even *m* values.

The two possible polyhedral arrangements: The detailed structure of the even m members of the MPTBp series is known up to $m = 12$. Among the six compounds ($m = 2, 4, 6, 8, 10$ and 12), only the modulated structure of $P_4W_{20}O_{68}$ ($m = 10$) does not possess orthorhombic symmetry at room temperature (Table 1). However, it should be noted that $P_4W_{24}O_{80}$ ($m = 12$) is known at room temperature in two forms: the first exhibits a modulation with a monoclinic lattice, the second is orthorhombic with space group $P2_12_12_1$ (Roussel, Mather *et al.*, 1998), which seems to be the high-temperature form ($T > 500$ K) quenched at room temperature. It is quite probable that the studied phase of $P_4W_{20}O_{68}$ ($m = 10$) (Roussel, Labbé, Leligny *et al.*, 2000) is a room-temperature form and there also exists an orthorhombic high-temperature form. This hypothesis is supported by an experiment described by Ottolenghi & Pouget (1996). Heating a monoclinic twinned crystal of $P_4W_{20}O_{68}$ from room temperature up to 450 K results in an untwinned crystal with orthorhombic symmetry. Consequently, one can envisage that for each even m member of the MPTBp series, there exists a high-temperature form which is orthorhombic and a low-temperature form, at $T < T_c$, with a more complex structure consisting of a small lattice distortion and lower symmetry.

The orthorhombic symmetry of all the even m members of this series results from the building principle of the structure:

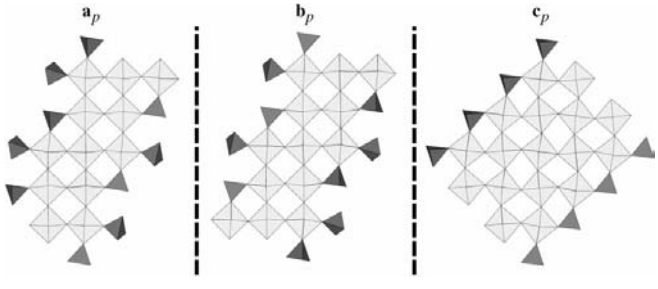

Figure 15
WO_6 octahedral tilting in the MPTBp series. Note that tilting of the WO_3 framework occurs only about the $\mathbf{c}_p$ direction.

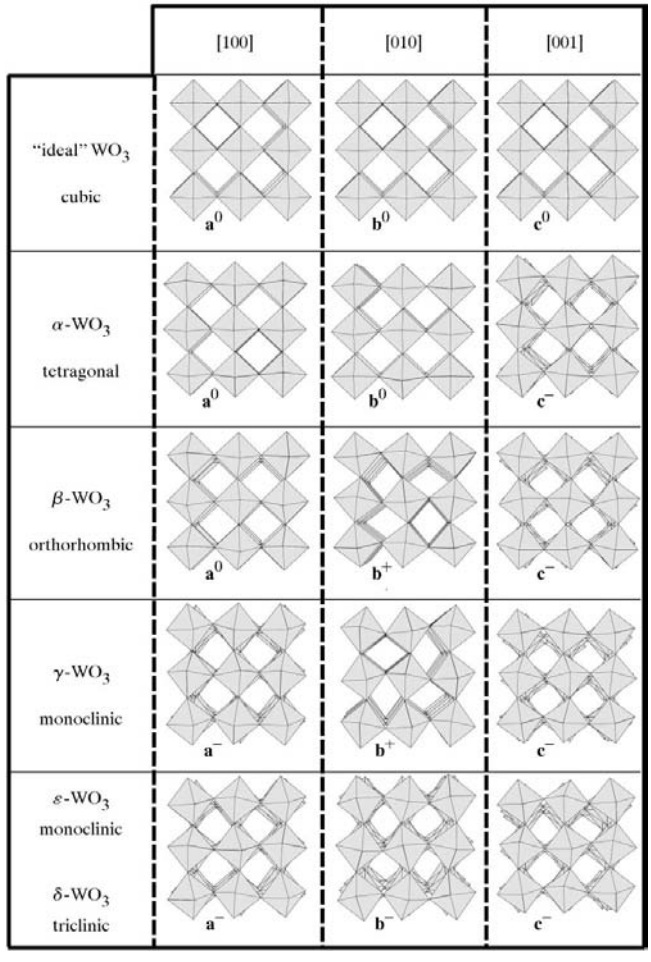

Figure 16
Tilt patterns observed in the different polymorphs of WO_3.

the succession of segments of $m/2$ WO_6 octahedra comprises a chevron-type arrangement through the isolated PO_4 tetrahedra. What symmetry can we expect for all these members? One should take into account both the connection between two adjacent slabs and the tilting mode of each slab. First, suppose there is no tilting. The ideal model is then reduced to a more simple arrangement in which each supposedly regular octahedron is lying on an edge (Fig. 17). The space group relative to such a hypothetical arrangement is centrosymmetric ($P2_1/m\ 2_1/c\ 2_1/n$). However, the tilting mode actually deletes, at least, both of the mirrors parallel to the projection plane and also the symmetry centres in such a way that only two acentric subgroups are possible: $P2_1cn$, effectively observed for $P_4W_4O_{20}$ ($m = 2$) (Wang, Wang & Lii, 1989), and $P2_12_12_1$, observed for the $m = 4$, 6, 8 and 12 members. This process is described in detail elsewhere (Roussel, Labbé & Groult, 2000). Now, what is the structural difference between these two arrangements corresponding to two different space groups? The easiest way to understand the change in the octahedral tilt system is to view the octahedral representation down the direction of a segment of $m/2$ WO_6 octahedra in a given slab, and to continue in the next slab through a PO_4 tetrahedron. Let us consider the (100) projection of the $P_4W_{12}O_{44}$ ($m = 6$) structure (Labbé *et al.*, 1986; Fig. 18). In a polyhedral chain, the octahedral tilt is, say, clockwise; in the adjacent slab, the extension of the chain at the same x level is always clockwise, as illustrated in the magnifying ellipse. For such an assembly, the space group is $P2_12_12_1$. On the contrary, if in the next slab the octahedral chain is counterclockwise (illustrated in Fig. 19), the space group becomes $P2_1cn$. This latter space group also exists in γ-Mo_4O_{11}, a structural MPTBp counterpart of the $m = 6$ member in which W and P are substituted for Mo (Ghedira *et al.*, 1985).

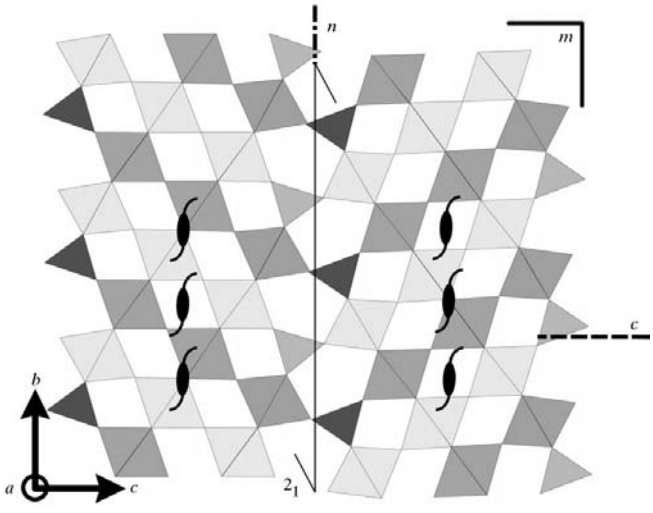

Figure 17
(100) projection of the idealized structure (*i.e.* without tilting) of $P_4W_{12}O_{44}$ ($m = 6$).

Thus, among the even m members of the MPTBp family, there are two possibilities of connection between two adjacent slabs, according to the tilt mode of the second slab with respect to the first one. Note again that this connection takes place at the level of O atoms common to both a PO_4 tetrahedron of a slab and to a WO_6 octahedron of the next slab. The tilt mode of the second slab may be 8° clockwise or −8° counterclockwise, for a given octahedral segment also implying the corresponding rotation of the PO_4 tetrahedra bound to three octahedra. However, this rotation does not change the position of the O atoms allotted to the connection between the two slabs. Thus, the tilting mode from one slab to the next does not influence the symmetry of the lattice. The remarkable fact is that the two connecting processes are actually observed within these crystal structures without any distortion of the lattice, which remains orthorhombic without a change in the cell parameters for a given m value.

The twin mechanism: The two possible subgroups obtained for the tilted structures are hemihedral: they possess half the symmetry elements of the group relative to the ideal untilted model. Consequently, for each of them, there exists a complementary structure corresponding to its image obtained using a symmetry element of the group, which does not exist in the subgroup. As an example, let us consider a structural block (A) of an even m term of the MPTBp family in $P2_12_12_1$ and its

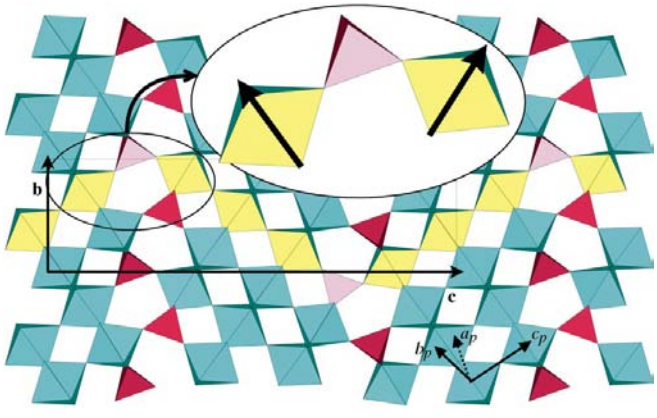

Figure 18
Type of tilting observed in $P_4W_{12}O_{44}$ ($P2_12_12_1$). In a chain of polyhedra (represented in yellow), the tilting (symbolized by arrows) always takes place in the same direction.

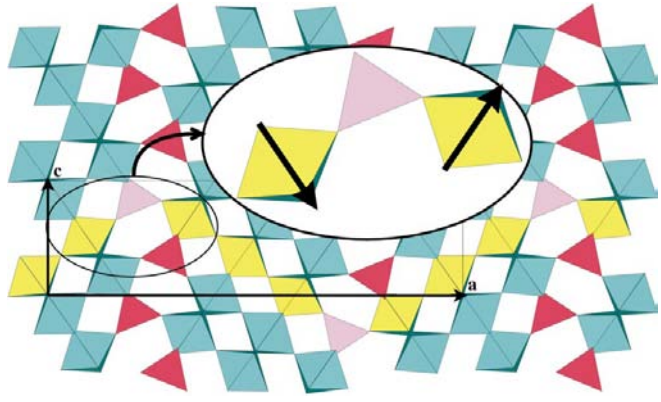

Figure 19
Type of tilting observed in γ-Mo_4O_{11} ($P2_1cn$). In a chain of polyhedra, the direction of tilting is reversed from one layer to the other

image (B) through any inversion operation, say using the (100) reflection plane. These two blocks have the same symmetry, but they are not superimposable: (A) and (B) are two enantiomorphous complementary components which correspond through an inversion, mirror or centre of symmetry (as two equivalent rhombic tetrahedra). However, these two structures have not been encountered separately. From the structure determinations, the differences are only important for a limited number of reflections for which the anomalous dispersion is sensitive. Some tests have been performed to that effect using classical wavelengths and substituting (x, y, z) coordinates by ($\overline{x}$, $\overline{y}$, $\overline{z}$), in order to obtain the absolute configuration (Roussel, Mather *et al.*, 1998).

However, the mixing of the two enantiomorphous structures within a unique sample seems the most probable. As the two components correspond to structural blocks for which the general tilting mode is reversed, the connection may be performed without difficulty at the level of a tetrahedral plane, since it is realised naturally in the structures which have the $P2_1cn$ space group as seen above. The 'pentagonal' tunnels are then maintained. However, another possibility exists in the connection process (Ghedira *et al.*, 1985) with the introduction of 'hexagonal tunnels' such as those found in the MPTBh family. This hypothesis supposes another fault in the stacking process at the level of a tetrahedra plane, which has been effectively observed in some micrographs (Fig. 20). The regular order of the octahedral segments as a chevron-type is then no longer maintained. The complementary structure of $P_4W_4O_{20}$ (m = 2) (Wang, Wang & Lii, 1989) with space group $P2_1cn$ may be obtained using either a symmetry centre, a mirror (100) or a twofold axis parallel to **b** or **c**. A schematic representation of the different tilting modes in the successive slabs of the structure (Fig. 21) gives a general idea of the possible connections at the level of the tunnels in the even m terms of the MPTBp structures.

3.1.4. Members with odd *m* values.

The two possible polyhedra arrangements: The detailed structures of the odd m members of the MPTBp series, which contain a regular succession of slabs of the same thickness, are known for $P_4W_{10}O_{38}$ (m = 5), $P_4W_{14}O_{50}$ (m = 7) and $P_4W_{18}O_{62}$ (m = 9). Moreover, the lattice symmetry is also known for $P_4W_{22}O_{74}$ (m = 11) and $P_4W_{26}O_{86}$ (m = 13) (see Table 1). As the polyhedral building arrangement is exactly the same for the odd m members as for the even m members, orthorhombic symmetry could be expected. However, they are either monoclinic or triclinic! The only structural difference is nevertheless minimal: inside a WO_3-type slab the shortest segments are now built alternately of (m + 1)/2 and (m − 1)/2 WO_6 octahedra. This small modification implies a total change in the symmetry, due to a distortion of the orthorhombic lattice which generates the systematic existence of twins. The presence of doublet spots in the diffraction patterns confirms that at least one cell angle differs from 90°.

Let us consider, as for the even m members, a hypothetical structure of an odd m member in which all the slabs are of ReO_3-type and therefore not tilted. The space group of this ideal model, where all the octahedra are lying on an edge, is $P2/m\ 2_1/n\ 2_1/n$, hence a centrosymmetric orthorhombic group (Fig. 22). There are two main differences between the ideal group of the even m terms ($Pmcn$) and that of the odd m terms ($Pmnn$). Firstly, the c-glide plane normal to **b** is substituted by an n plane; this change is only due to a translation **a**/2 of the segments including either (m + 1)/2 or (m − 1)/2 WO_6 octahedra into two successive slabs. Secondly, the twofold axes parallel to **a**, located in the central plane of a slab, are not the same in both structure types. In the even m members, the screw axes (2_1) are located outside a segment of m/2 octahedra (Fig. 17). Conversely, in the odd m members, the twofold rotation axes are located in the middle of a segment (Fig. 22). In both cases, the m mirrors normal to **a** imply that the symmetry centres are located in the diads 2 and 2_1. The influence of tilting upon an odd m member is then illustrated in Fig. 23. As previously, the tilt of a segment, and consequently the correlated tilt of all the segments in a slab, involve the loss of the m mirrors. Therefore, contrary to the even m members, the twofold axes are no longer suitable, whereas the symmetry centres continue to exist. Two monoclinic centrosymmetric subgroups (index 2) of $Pmnn$ become

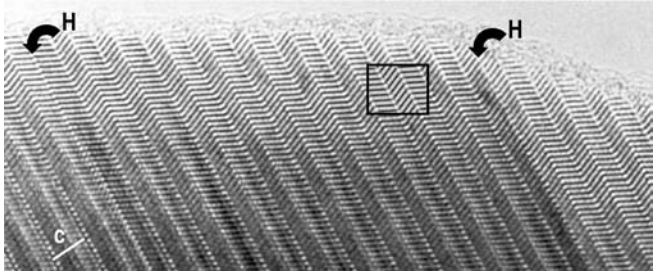

Figure 20
[110] HREM image of a crystal of $P_4W_{14}O_{50}$ showing two rows of hexagonal tunnels (H) in a MPTBp matrix.

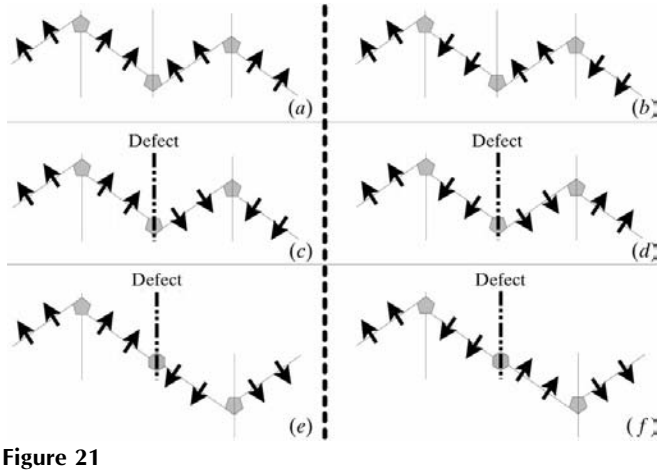

Figure 21
Various modes of tilting encountered in the MPTBp series: (*a*) m = 6 type ($P2_12_12_1$): the tilting direction is identical from one layer to the other; (*b*) m = 2 type ($P2_1cn$): the tilting direction is reversed from one layer to another; (*c*) and (*d*) influence of a defect (mirror): locally, the junction is identical to that observed naturally in the m = 2 type (*c*) or in the m = 6 type (*d*); (*e*) and (*f*) defect (hexagonal tunnel): the junction is identical to that observed naturally in the MPTBh family.

possible: $P2_1/n$ with **b** as a unique axis and $P2_1/n$ with **c** as a unique axis. These two groups are observed: the first for $P_4W_{10}O_{38}$ ($m = 5$; Roussel, Drouard *et al.*, 1999) and for $P_4W_{14}O_{50}$ ($m = 7$; Roussel *et al.*, 1996) and the second for $(Mo,W)_9O_{25}$ (d'Yachenko *et al.*, 1995; Kihlborg *et al.*, 1994) isostructural with $P_4W_{14}O_{50}$ ($m = 7$), in which the tetrahedral sites are all occupied by Mo atoms, whereas octahedral sites are mixed (Mo, W). A subgroup of greater index as $P\overline{1}$ is also encountered in $P_4W_{18}O_{62}$ ($m = 9$) (Roussel, Labbé & Groult, 2000).

So, the simultaneous existence of octahedral segments with different lengths inside a given slab of WO_3-type, as well as the elaboration of a tilting mode for the WO_6 octahedra, induce distortions of the orthorhombic lattice and lead to a lower symmetry: either monoclinic or triclinic. This distortion remains weak: the lattice angles are close to a right angle, often ~90.2° and up to 90.4° for $m = 5$. However, always with the same structural type, the two monoclinic examples in $P2_1/n$ can be found either with **b** or **c** as the unique axis, the distortion taking place either in the **ac** plane for the odd m members of the MPTBp's, also including $m = 9$, or in the **ab** plane for the mixed (Mo, W) compound.

The obvious questions are: 'what is the difference between these two structural types and what is the mechanism which induces the distortions?'. The answers are again provided by the connection between two successive tilted slabs. Consider, for example, a projection (100) of $P_4W_{14}O_{50}$ ($m = 7$; Fig. 24; Roussel *et al.*, 1996). A zigzag polyhedral chain along **c** at a given x level is composed of four octahedra, one tetrahedron, three octahedra, one tetrahedron *etc.* If one travels along such a chain it can be observed that all the octahedra are tilted (~8°) in the same direction. The generated space group is $P2_1/n$ with **b** as the unique axis. However, if we now contemplate the second possibility of tilting for the second slab, reversed from one slab to the other (Fig. 25), so the structure becomes that of $(Mo,W)_9O_{25}$ (d'Yachenko *et al.*, 1995), retaining the space group $P2_1/n$, but now with the long axis **c** as the unique axis.

The twin mechanism: Very frequently, pseudosymmetries give rise to twin phenomena and the odd m members of the MPTBp family provide a good illustration. For all diffraction patterns realised with this class of crystal, a splitting of the reflections is always observed. The distribution of double spots on films or of double peaks in profile studies leads to the unambiguous conclusion that in a given sample, two identical symmetrically distributed structural domains systematically exist. We will see that the models deduced from these observations are again closely related to the tilting of the octahedral segments, but also to the relative spatial orientation of the two symmetrical domains. For all these odd m members, the twin law is consistent with two blocks whose **a** and **b** parameters are merged, whereas the two **c** vectors include a small angle (Table 1): 0.80° in $P_4W_{10}O_{38}$ ($m = 5$), 0.38° in $P_4W_{14}O_{50}$ ($m = 7$) and 0.40° in $P_4W_{18}O_{62}$ ($m = 9$).

One can use an argument identical to that already proposed before for the even m members, relying on the projection of $P_4W_{14}O_{50}$ ($m = 7$) in Fig. 24. This monoclinic structure has space group $P2_1/n$ with **b** unique. If we apply to it one of the symmetry operations of the hypothetical group $P2/m\ 2_1/n\ 2_1/n$, which does not exist in the subgroup, *i.e.* if we apply either the twofold axes parallel to **a** and **c** or the mirrors parallel to **bc** and **ab**, an image of the structure is again

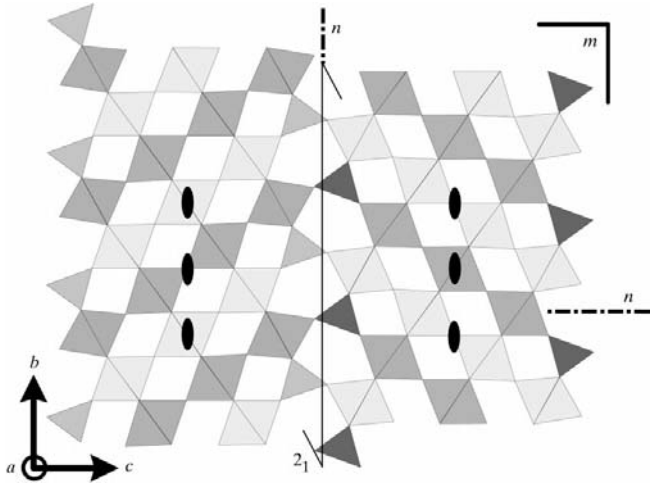

Figure 22
(100) projection of the idealized structure (*i.e.* without tilting) of $P_4W_{14}O_{50}$ ($m = 7$), taken as an odd example.

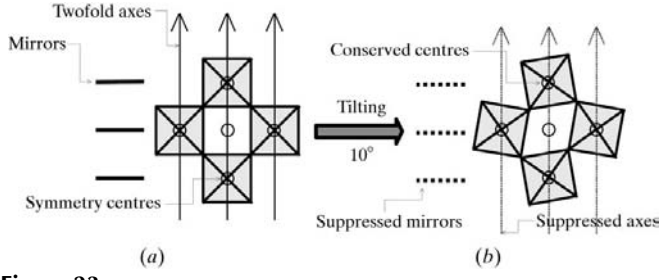

Figure 23
Schematic representation of the WO_6 octahedra in an idealized structure without tilting (*a*) and in the actual structure (*b*) for the $m = 7$ member.

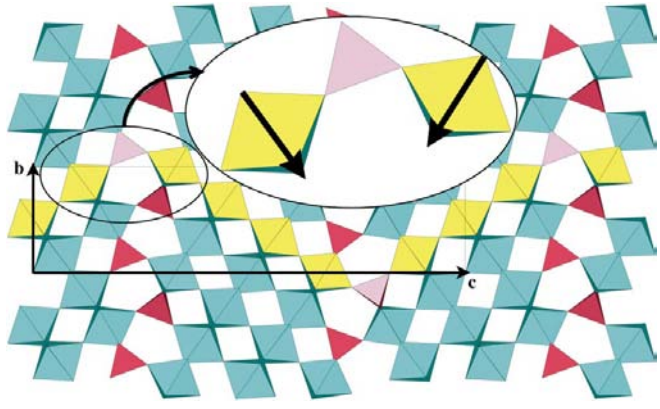

Figure 24
Type of tilting observed in $P_4W_{14}O_{50}$ (space group $P2_1/n$, unique axis **b**). In a chain of polyhedra (represented in yellow), the tilting (symbolized by arrows) always takes place in the same direction.

obtained with a general reverse tilting effect for all the slabs but which presents two major differences from the even m cases. First, the image which preserves the $P2_1/n$ space group preserves the tilting orientation since the structure is centrosymmetrical; this means that the two structural models are now strictly superimposable. Secondly, these two models are oriented symmetrically with respect to the twin **ab** plane, which is the common plane here, *i.e.* the original composition plane. Again, indeed, the two components of the twin can be easily connected through the O atoms of the PO_4 tetrahedra located in a (001) slice. As previously, this plane is a favoured plane to initiate the reverse tilting mode, since it is generated naturally in the structure including (Mo,W) mixed sites. This phenomenon can be repeated several times during the growth process generating a twin.

Keeping in mind the previous argument, one also expects to find the twin phenomenon in the mixed (Mo,W) compound which is the counterpart of $P_4W_{14}O_{50}$ (m = 7), also with the space group $P2_1/n$, but now with **c** unique. However, this compound is not reported as being twinned (d'Yachenko *et al.*, 1995). An explanation of this fact can still be deduced from the polyhedral models. The image of this structure (Fig. 25) may be generated by a twofold axis parallel to **a** or **b**, or by the **ac** or **bc** planes. Moreover, the related orientation of the two components is important. Contrary to the previous case, in which γ was strictly 90°, this angle is now different from a right angle so that in the (001) plane, which remains the original composition plane, their mutual orientation induces unbearable mechanical strains. For example, a twofold axis along **a** keeps the orientation of **a** and **c** unchanged, but causes a non-negligible angle between **b** and its image **b**′. Its value would be 0.36° in $(Mo,W)_9O_{25}$. The distribution of the O atoms of the PO_4 tetrahedra in a given (001) plane is not able to ensure a connection between the two symmetrical components without a major distortion and consequently the twin is not initiated during the growth process.

The particular situation of $P_4W_{18}O_{62}$ (m = 9): The previous considerations relating to the absence of twinning in $(Mo,W)_9O_{25}$ (d'Yachenko *et al.*, 1995), for which $\gamma \neq 90°$, seems in complete contradiction with the existence of twinning in the triclinic phase $P_4W_{18}O_{62}$ (m = 9) (Roussel, Labbé & Groult, 2000), in which γ = 89.78°. Indeed, the twin law in $P_4W_{18}O_{62}$ is exactly the same as that found for $P_4W_{10}O_{38}$ (m = 5) (Roussel, Foury *et al.*, 1999) and for $P_4W_{14}O_{50}$ (m = 7; Roussel *et al.*, 1996) and at first sight, the twin effect seems paradoxical. However, all depends again on the sequence of the successive tilted slabs of WO_3-type. It has been verified that, although it is triclinic, the m = 9 member involves an arrangement of the adjacent slabs relative to the linking of the successive tilted segments, which is completely analogous to that observed in m = 5 and in m = 7. Consequently, its image through a mirror such as a (001) plane, which consists of the reverse tilting of all the WO_6 octahedra, has exactly the same **a** and **b** vectors. The fact that these vectors are not perpendicular does not influence the twin law and (001) remains both the twin plane and the original composition plane. This condition cannot be assumed to be met in $(Mo,W)_9O_{25}$, because the (001) symmetry plane is already present in its space group.

The measurements of the cell parameters of the MPTBp series and particularly of the β angles of the monoclinic members (m = 5 and m = 7) and the three angles of the triclinic member (m = 9) are complex because of the pseudo-orthorhombic character of the cell and of the existence of twins. However, these measurements were achieved using

(i) the unsplit reflections $hk0$ in the original plane (001)*, which is, in the reciprocal lattice, the common plane of the two symmetrical components, and

(ii) few reflections outside (001)*, for which only one of the two expected split components hkl and $\bar{h}kl$ appears because the other is very weak, with a structure factor close to zero.

The rigorous indexing of such rather rare reflections detected in the patterns permitted the determination of the cell parameters unambiguously with a small standard uncertainty. It arises from this process that the triclinic cell of $P_4W_{18}O_{62}$ (m = 9) was precisely determined with α confused with a right angle 90.00 (2)°, but with β equal to 90.20 (2)° and γ equal to 89.78 (2)°.

3.1.5. Concluding remarks. The main feature which characterizes all the members of the MPTBp series is the tilt phenomenon of the WO_6 octahedra along a segment. The regular stacking of tilted slabs of WO_3-type may be performed in two ways for even m, and two ways for the odd m members, leading to four different structure types. The two polyhedral arrangements generated for the even m members are orthorhombic hemihedral and each of them generates a merohedral twin with an original composition plane confused with the twin plane (001). The two orthorhombic lattices are thus merged, giving rise to a single orientation of the reciprocal lattice and hence single diffraction spots. The two polyhedral arrangements generated for the odd m members are monoclinic or triclinic and only one of them generates a possible pseudo-symmetric twin. The lattices are then distinctly oriented, giving rise generally to split diffraction spots. In all cases it seems that the twins are contact twins which are polysynthetic on a microscopic scale.

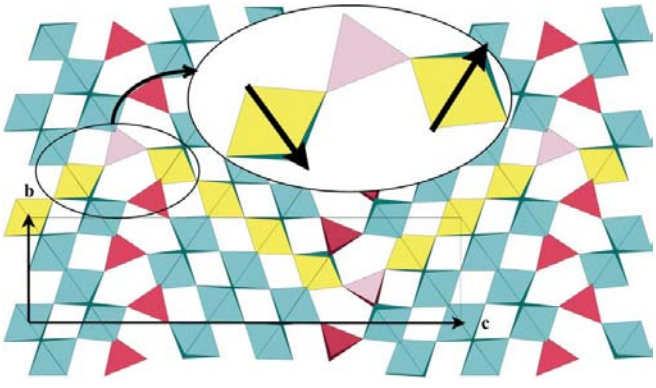

Figure 25
Type of tilting observed in $(Mo,W)_9O_{25}$ (space group $P2_1/n$, unique axis **c**). In a chain of polyhedra, the direction of tilting is reversed from one layer to the other.

Table 2
The MPTBh series.

m	Formula	a (Å) α (°)	b (Å) β (°)	c (Å) γ (°)	Space group	References
4	$K_{0.84}P_4W_8O_{32}$	6.6702 (5) 90	5.3228 (8) 100.546 (7)	8.9091 (8) 90	$P2_1/m$	(*a*), (*b*) (*c*), (*d*) (*e*), (*f*)
4	$Na_{1.5}P_4W_8O_{32}$	6.6075 (5) 90	5.277 (4) 99.64 (5)	17.788 (11) 90	$P2_1/c$	(*g*), (*h*) (*i*), (*j*)
6	$K_{2.01}P_4W_{12}O_{44}$	6.6736 (2) 90	5.3543 (3) 92.615 (3)	11.9005 (5) 90	$P2_1/m$	(*b*), (*k*)
6	$Na_{1.7}P_4W_{12}O_{44}$	6.588 (2) 90	5.291 (1) 93.47 (4)	23.775 (17) 90	$P2_1/c$	(*g*), (*h*) (*i*), (*j*)
7	$K_{1.4}P_4W_{14}O_{50}$	6.660 (2) 90	5.3483 (3) 97.20 (2)	27.06 (5) 90	$A2/m$	(*l*), (*b*)
7	$Na_{1.7}P_4W_{14}O_{50}$	6.575 (2) 89.62 (1)	5.304 (1) 96.17 (1)	27.076 (3) 90.26 (1)	$A\bar{1}$	(*m*), (*j*)
7	$Pb_{0.66}P_4W_{14}O_{50}$	6.6015 (3) 90.208 (6)	5.3156 (4) 96.757 (5)	27.039 (2) 89.867 (5)	$A\bar{1}$	(*n*)

References: (*a*) Giroult *et al.* (1982*a*); (*b*) Domengès *et al.* (1988); (*c*) Roussel *et al.* (1997); (*d*) Dumas *et al.* (1999); (*e*) Drouard *et al.* (1999); (*f*) Drouard *et al.* (2000); (*g*) Benmoussa, Groult & Raveau (1984); (*h*) Benmoussa, Labbé, Groult & Raveau (1982); (*i*) Wang, Greenblatt, Rachidi, Canadell & Whangbo (1989*a*); (*j*) Domengès *et al.* (1990); (*k*) Roussel, Drouard *et al.* (1999); (*l*) Domengès, Goreaud *et al.* (1983); (*m*) Lamire *et al.* (1987*a*); (*n*) Roussel, Masset *et al.* (1998).

3.2. Monophosphates with inserted cation $A_x(PO_2)_4(WO_3)_{2m}$ (A = Na, K, Pb)

3.2.1. The MPTBh family.

Symmetries in the MPTBh series: Seven detailed single-crystal X-ray diffraction studies are known at room temperature (Table 2): three compounds with K and three with Na as inserted cations (m = 4, 6 and 7), and only one with Pb (m = 7). However, the cell parameters of five different lead compounds isolated as pure phases (m = 6, 7, 8, 9 and 10) were measured using powder diffraction data (Roussel, Masset *et al.*, 1998). All these structures are built according to the same principles as described in §2: a regular stacking of WO_3-type slabs all of the same thickness, but now having the same orientation, so that segments of WO_6 octahedra in successive slabs are now parallel and no longer show the chevron arrangement. At the interface of these slabs, a set of pseudo-hexagonal tunnels are gathered along a slice parallel to the slabs (Fig. 7). The basic arrangement is therefore monoclinic, as found for five members out of seven, the last two being triclinic. Consequently, the twofold axis was chosen along **b** (Giroult *et al.*, 1982*a*), with the **b** axis being ∼5.30 Å, which is twice the edge length of a WO_6 octahedron. This parameter was called a in the MPTBp family. The c parameter remains the longest parameter and lies obliquely through the slabs. Examination of Table 2 prompts two remarks: (*a*) there is again a great diversity in the symmetries of the structural arrangements since four different space groups are encountered, and (*b*) the c parameters are the same for Na and Pb compounds for a given m, but is halved for some of the K compounds. The reason for this diversity is again related to the polyhedral tilting modes.

Tilting modes: The tilting mode observed in the MPTBh family $A_x(PO_2)_4(WO_3)_{2m}$ is a little more complex than that encountered in the MPTBp family. Indeed, the A cation type plays a non-negligible part in the WO_6 octahedral tilting process. An inserted cation such as Na^+ or Pb^{2+} generates a tilting mode similar to that encountered in all members of the MPTBp family, therefore, a type ($a^0b^0c^+$) in Glazer's (1972) notation. On the contrary, for the potassium compounds the WO_6 octahedra are not tilted at all (Fig. 26), leading to the notation ($a^0b^0c^0$). It has been found that the size and shape of the inserted cation in the hexagonal tunnels influence the tilt amplitude with respect to the untilted structure (Roussel, Masset *et al.*, 1998). In the Na compound the tilt angle is ∼8.5° as in all members of the MPTBp family. The same angle is slightly reduced to 6.5° when Pb is introduced, but it is zero for the three K compounds (m = 4, 6 and 7). Therefore, the size of K ions may serve to align all the octahedra. There is, however, another hypothesis (Benmoussa, Groult, Labbé & Raveau, 1984) which supposes the existence of two forms for each compound, a low-temperature form which is tilted and a high-temperature form which is not tilted. At room temperature, the Na and Pb compounds should be low-temperature forms, whereas all K compounds should be high-temperature forms. This hypothesis is yet to be verified and the influence of the ratio of inserted cations is not confirmed either.

How is it possible to understand the occurrence of symmetries observed at room temperature? Consider first the even m members (m = 4, 6). The untilted models corresponding to the K compounds contain segments of $m/2$ straight WO_6

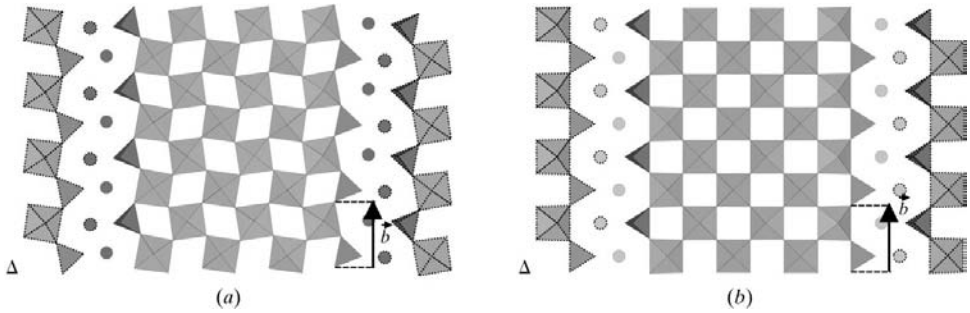

Figure 26
Various modes of tilting in the MPTBh series: (*a*) in the compounds containing sodium and lead: ($\mathbf{a}^0\mathbf{b}^0\mathbf{c}^+$) type; (*b*) in the compounds containing potassium: ($\mathbf{a}^0\mathbf{b}^0\mathbf{c}^0$) type.

octahedra in each slab and hence all the slabs are equivalent through a lattice translation t. The c parameter is directly related to the thickness of a slab ($c \times \sin\beta$); its values are 8.9 and 11.9 Å, respectively, for $m = 4$ (Giroult *et al.*, 1982*a*) and $m = 6$ (Roussel, Drouard *et al.*, 1999). The arrangement of all the polyhedra is according to the space group $P2_1/m$. In the Na and Pb compounds all the $m/2$ octahedra of a segment are tilted in the same direction, as in the MPTBp family, but the previous t translation now connects two different tilted segments, one clockwise and the other counterclockwise (Fig. 27). This fact was observed systematically. The c parameter is consequently twice that of the related K compounds and once more, the m mirrors are discarded and replaced by a **c** glide plane, the corresponding group becoming $P2_1/c$. Consider now the odd ($m = 7$) members. Each slab now contains segments built of 3 [*i.e.* $(m-1)/2$] and 4 [*i.e.* $(m+1)/2$] WO_6 octahedra, but in two successive slabs two identical segments are now shifted from **b**/2. As the atomic arrangement is always monoclinic, the best choice is the retained monoclinic cell with $\mathbf{c} \simeq 27$ Å (Table 2), which becomes an A-centred cell. For the K compound (Domengès, Goreaud *et al.*, 1983), the space group $A2/m$ is according to the untilted polyhedral arrangement (Fig. 28), which preserves only the symmetry centres to become $A\bar{1}$ in Na compounds (Benmoussa, Groult & Raveau, 1984) and Pb compounds (Roussel, Masset *et al.*, 1998), where the octahedra are tilted (Fig. 29).

The three $m = 7$ compounds have similar lattices, monoclinic or pseudo-monoclinic, with a c parameter of ~27 Å. However, some of the diffraction patterns show clearly a doubling of the c parameter. Consider a schematic representation of the $h0l$ reciprocal plane (Fig. 30). It can be viewed as a twin phenomenon due to a metric coincidence $a^* \sin(\pi/2 - \beta^*) = c^*/2$ or in direct space $\beta = \arccos(-a/2c)$, which is verified for $\beta = 97°$, precisely the observed value. This new twin may be classified in the species twin-lattice quasi-symmetry (TLQS). The two components are related either through an **ab** plane or through a rotation of 180° about a twofold axis along **a**. In both cases, the connection may occur using the tetrahedra as achieved generally in the MPTBp family building a slice of pentagonal tunnels. This twin type also appears for other m values as in $K_xP_4W_8O_{32}$ ($m = 4$). More complex arrangements are discovered by electron diffraction, for example (Figs. 31 and 32) with a sample of $Pb_xP_4W_{12}O_{44}$ ($m = 6$) (Roussel, Masset *et al.*, 1998).

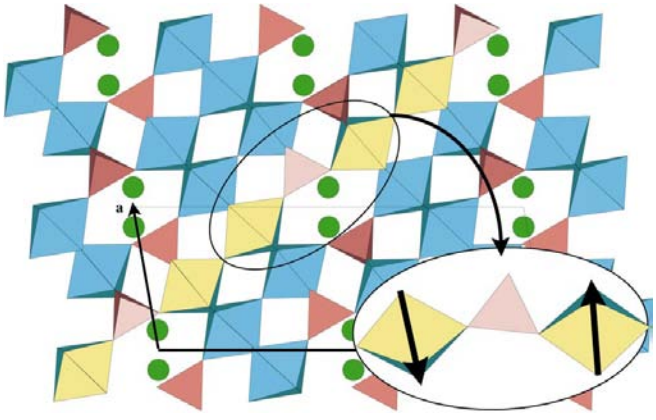

Figure 27
Type of tilting observed in $Na_xP_4W_8O_{32}$. In a polyhedral chain, the direction of tilting is reversed from one layer to the other.

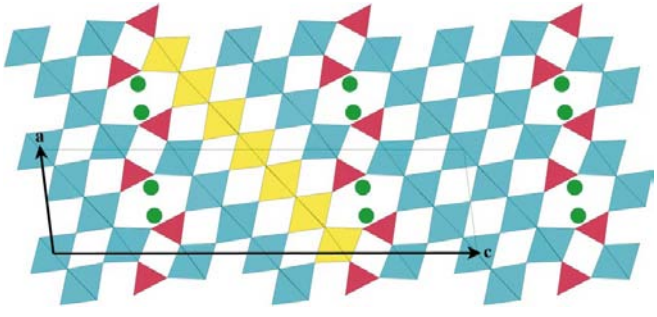

Figure 28
(010) projection of $K_xP_4W_{14}O_{50}$ (space group $A2/m$): no tilting of the octahedra is observed.

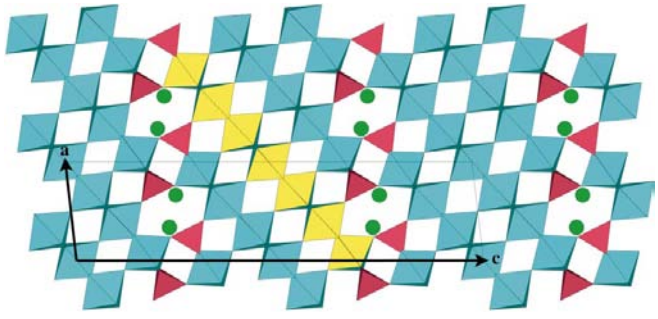

Figure 29
(010) projection of $Na_{1.7}P_4W_{14}O_{50}$ (space group $A\bar{1}$): the WO_6 octahedra are tilted.

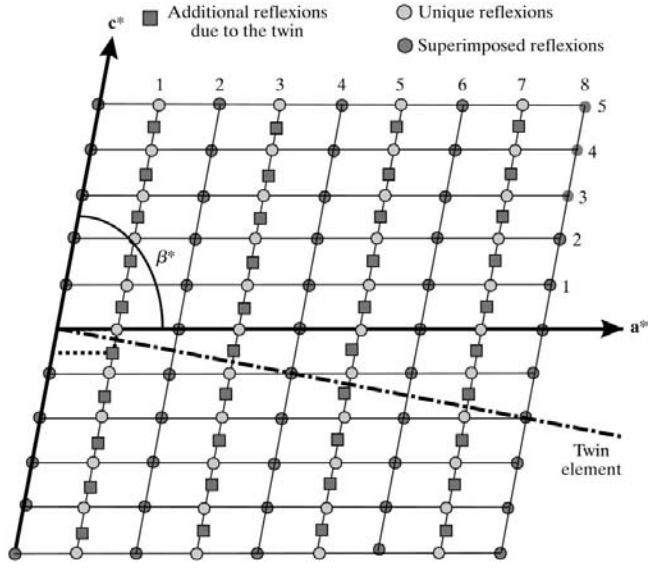

Figure 30
Schematic representation of the reciprocal space of a twinned crystal implying an apparent doubling of the cell.

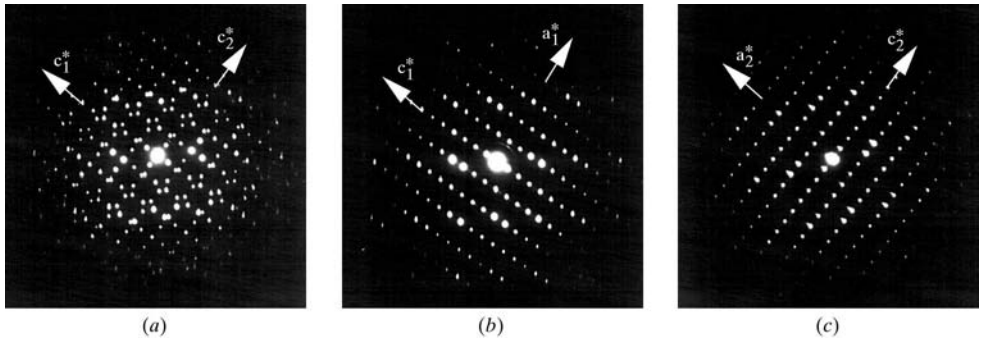

Figure 31
Electron diffraction pattern corresponding to the defect observed in $Pb_xP_4W_{12}O_{44}$ (shown Fig. 31): (*a*) both domains are superimposed; (*b*) and (*c*) first and second domain, respectively.

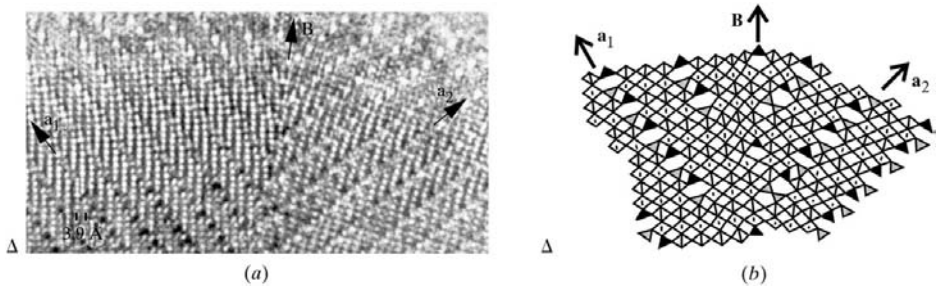

Figure 32
Defect observed in $Pb_xP_4W_{12}O_{44}$: (*a*) HREM image showing two domains and their junction; (*b*) theoretical model using WO_6, PO_4 and P_2O_7 polyhedra to explain the junction between the domains.

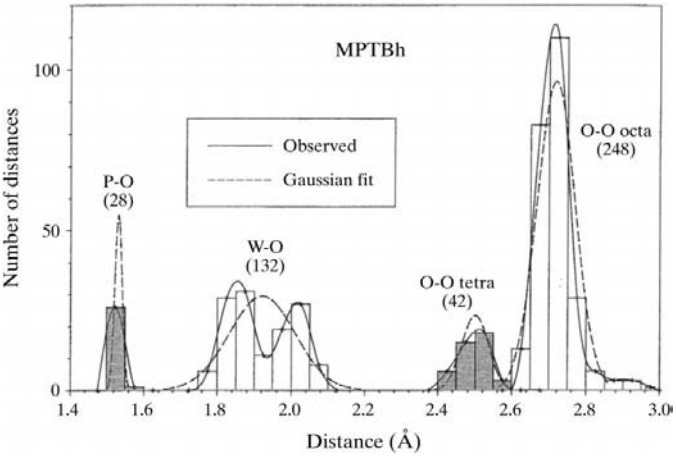

Figure 33
Histogram of the interatomic distances in the MPTBh series. Shaded areas are related to PO_4 tetrahedra.

Interatomic distances and mixed valence of W atoms: The seven structures solved by single-crystal X-ray diffraction (Table 2) are known precisely. A total of 290 independent O—O distances were collected, 42 of which belong to the PO_4 tetrahedra and 248 to the WO_6 octahedra. A histogram of the interatomic distances in the polyhedra (Fig. 33) shows that the P—O and O—O distances in each polyhedron form a Gaussian distribution with a maximum corresponding to the mean of the observed distances: d_{P-O} = 1.53 (1), $d_{O-O\ tetra}$ = 2.50 (4), $d_{O-O\ octa}$ = 2.72 (5) Å; on the other hand, the W—O distances show two peaks located at 1.86 and 2.02 Å, the average of the 132 W—O distances being 1.92 (9) Å. This bimodal distribution of W—O distances is explained if one takes into account the geometrical influence of the lateral PO_4 tetrahedra in a slab upon the dispersion of the interatomic distances observed in the octahedra. Thus, in the WO_6 octahedron furthest from the middle of the slab, *i.e.* the nearest of a tetrahedral slice, three long and three short W—O distances are observed. The related octahedron is then connected through O atoms to three tetrahedra and three octahedra. As the octahedron becomes closer to the middle of a slice, the W—O distances tend to progressively gather about the mean value of 1.92 Å when the octahedron is connected to six octahedra (Fig. 34). Thus, one notes a gradual deformation of the octahedra from the centre of the section towards the periphery. This fact is consistent for all seven structures (Lamire *et al.*, 1987*a*; Roussel, Masset *et al.*, 1998; Roussel, Drouard *et al.*, 1999).

The dispersion of the W—O distances can be correlated with the formal oxidation state of each tungsten ion. Indeed, the formal valence v of each atom can be evaluated, in a first approximation, using the Brown & Altermatt (1985) relation starting from the interatomic W—O distances: $v = \sum_{i=1}^{6}(R_i/R_0)^{-E}$, where R_i is the ith W—O distance and E a constant which depends on the types of involved atoms (E = 5.75 for W—O bonds and 4.29 for P—O bonds; Brown & Wu, 1976). R_o is an adjustment parameter (R_o = 1.917 for W^{6+} and O^{2-}). However, to be able to compare the results between them, it is necessary to normalize R_o (Domengès *et al.*, 1985) so that the sum of the formal valences of all the octahedra is equal to the total valence of the compound, deduced from the chemical formula, by applying the principle of the charge electroneutrality.

The evolution of the average number of conduction electrons calculated using the relation $n = 6 - v$ with respect to the W position is shown in Fig. 35 (Roussel, Drouard *et al.*, 1999). In this figure, a black square represents a P site and a grey circle a W site. The electron density is maximal in the centre of the layers, which seems to indicate that the conduction electrons are mainly confined in the medium of the conducting WO_3-type layers. The coupling between the elec-

trons belonging to two close layers must thus be weak, arising from the two-dimensional character of the compound.

3.2.2. Comparison with the MPTBp family. The studies of the ternary diagrams $K_xNa_y(PO_2)_4(WO_3)_{2m}$ reported previously show that there exists a small domain near $P_4W_8O_{32}$ and $P_4W_{12}O_{44}$ where Na atoms may enter the structure of monophosphate tungsten bronzes with pentagonal tunnels (MPTBp family). A single crystal of good quality was obtained with the composition $Na_{0.96}P_4W_{12}O_{44}$ (Roussel, Groult *et al.*, 1999). The orthorhombic structure, space group $P2_12_12_1$, has exactly the same polyhedral arrangement as in $P_4W_{12}O_{44}$ (Fig. 18), with only a very slight increase of the cell volume (< 1%).

The location of the Na sites in $Na_{0.96}P_4W_{12}O_{44}$ (Fig. 36) monophosphate tungsten bronzes with pentagonal 'tunnels' (MPTBp) may be compared with the location of cations in $Na_{1.7}P_4W_{12}O_{44}$ (Benmoussa, Groult, Labbé & Raveau, 1984; Fig. 37), monophosphate tungsten bronzes with hexagonal 'tunnels' (MPTBh). These 'tunnels' actually result from the existence of large O_{18} cages, bound by 18 O atoms, stacked along **a** and **b**, and which are interfaced with windows of different size and shape. In the MPTBp family, each O_{18} cage is related with four equivalent O_{18} cages through a pentagonal window (Fig. 36). In the MPTBh family, an O_{18} cage is related with four equivalent cages either through a large hexagonal window (Fig. 37) or through small diamond-shape windows bound by two octahedra and two tetrahedra. The mean plane of all these polygons is oriented 45° from the projection plane and true tunnels with an axis normal to the projection plane do not exist. Moreover, the area covered by these cages, which is represented in the previous figures as dashed elliptical lines, extends greatly beyond the layout of the windows.

The two O_{18} cages are drawn in Fig. 38. Both are surrounded with eight WO_6 octahedra and four PO_4 tetrahedra and have exactly the same extension. As seen in Fig. 38, the right parts of these two cages are the same, but the left parts are related to each other by a rotation over 180° about a horizontal twofold axis, the connection being made by four symmetrically equivalent O atoms, building a distorted rhombus labelled O(6*a*, 6*b*, 6*c* and 6*d*) in MPTBp and O(11*a*, 11*b*, 11*c* and 11*d*) in MPTBh. The shape and size of these two oxygen webs may be considered taking into account the O—O related distances, for example, O(1)—O(11) [MPTBp]

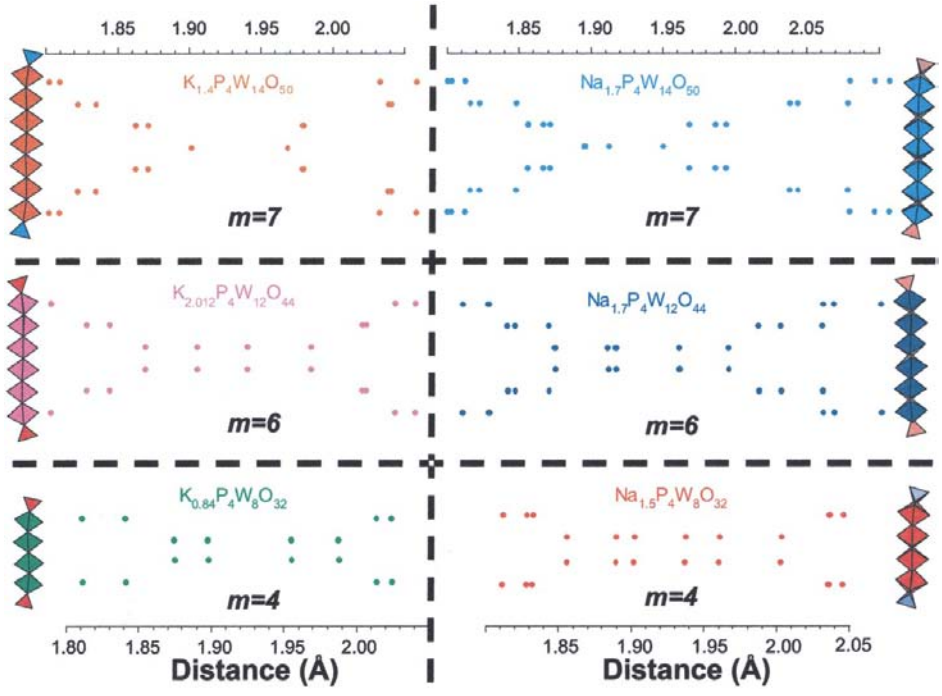

Figure 34
Dispersion of the W—O distances in the WO_6 octahedra in the MPTBh series.

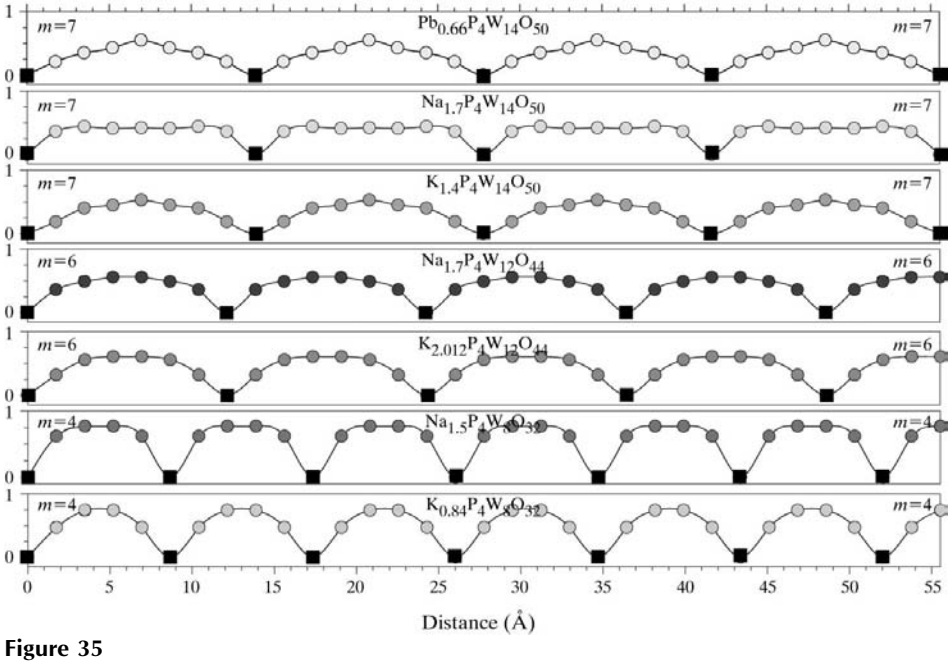

Figure 35
Number of conduction electrons per W atom in the MPTBh family. Note that this number is highest in the middle of the WO_3-type slab.

and O(2)—O(3) [MPTBh]. It appeared that the mean difference between the corresponding 36 O—O distances is only 1.6%. The similarity of both cages strongly suggests that the same Na^+ cation situated in an identical site should have a similar oxygen surrounding. However, the dispersion of the Na—O distances is very different. In the MPTBp compound, Na^+ is located 1.50 Å from the centre of the O_{18} cage (Roussel, Groult *et al.*, 1999); it results in an environment with seven short Na—O distances ranging from 2.37 to 2.64 Å and an eighth at 2.82 Å. Such a cation site seems perfectly suitable to Na, the shortest Na—O distance corresponding to the sum of the ionic radii (1.00 + 1.35) Å. Conversely, in the MPTBh compound Na is located 1.11 Å from the cage centre and adapts to an oxygen neighbourhood with four short distances (2.45–2.64 Å) and four longer ones (2.85–3.02 Å). In both cage types Na^+ is bound preferentially to O atoms of the PO_4 tetrahedra, since out of eight O atoms, six are atoms of the W—O—P bridges, whereas only two O atoms belong to two WO_6 octahedra.

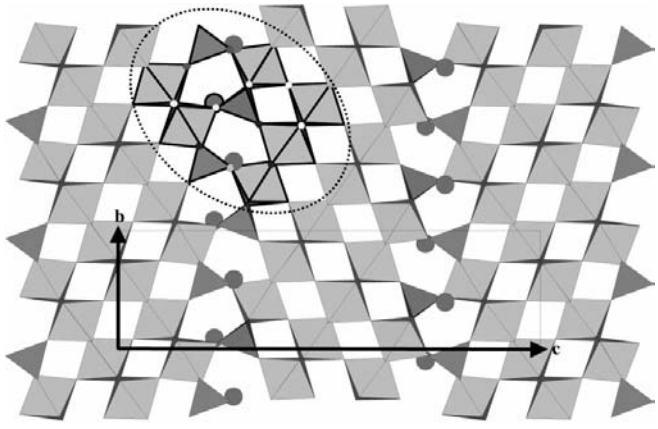

Figure 36
Projection onto (100) of the crystal structure of $Na_{0.96}P_4W_{12}O_{44}$, MPTBp-type. Polyhedra drawn with thick lines delimit the extension of O_{18} cages (dotted curves).

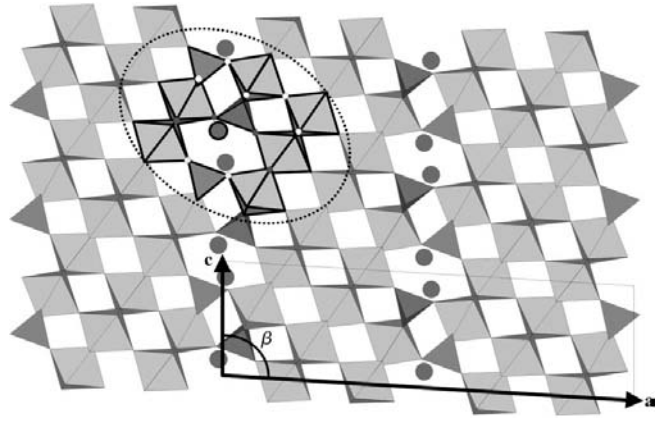

Figure 37
(010) projection of the crystal structure of $Na_{1.7}P_4W_{12}O_{44}$, MPTBh-type. Polyhedra drawn in thick lines delimit the extension of O_{18} cages (dotted curves).

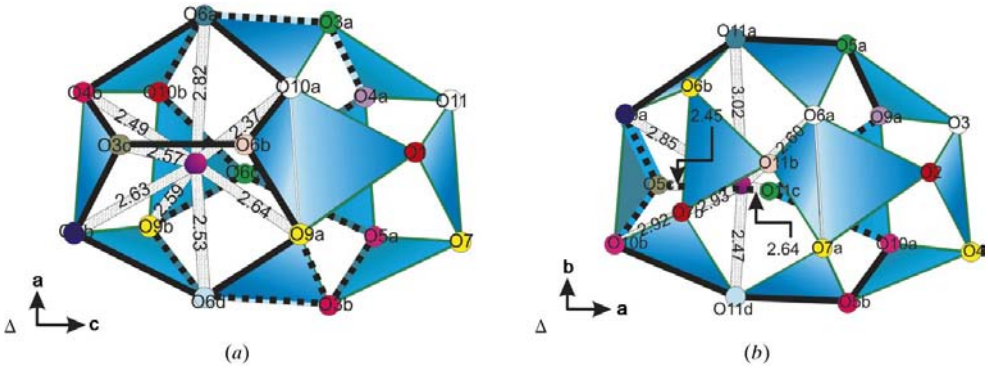

Figure 38
Location of the Na^+ cation inside an O_{18} cage in (*a*) MPTBp $Na_{0.96}P_4W_{12}O_{44}$ and (*b*) in MPTBh $Na_{1.7}P_4W_{12}O_{44}$.

The synthesis of an Na-doped MPTBp is quite recent (Roussel, Groult *et al.*, 1999). Roughly, it was thought that as the hexagonal tunnels appear larger than the pentagonal ones, it was logical to find cations inserted systematically into the hexagonal tunnels and to notice that the pentagonal tunnels were always empty. The study of the O_{18} cage topologies, showing that the cation sites were identical, urged the authors to try to insert some cations into the cages, although all the previous attempts had failed. Only the insertion of Na atoms was successful and only for $m = 6$. However, the fact that the occupation rate of Na seems limited to 1/4 is not currently explained.

4. Phase transitions in monophosphate tungsten bronzes

4.1. Instabilities and charge density waves

4.1.1. X-ray diffuse scattering observations. Low-dimensional metals can show several types of electronic instabilities (Schlenker *et al.*, 1989) tending to stabilize a charge density wave (CDW) or a spin density wave (SDW) state or a superconducting ground state. The CDW and superconductivity instabilities have been effectively observed in MPTBp's with the formula $(PO_2)_4(WO_3)_{2m}$. This family has been widely investigated in the phase-transitions area. Electron transport measurements as well as X-ray diffuse scattering investigations have shown the formation of several successive CDW transitions in all the members with $m \leq 14$, as well as the onset of superconductivity in the $m = 7$ members (Hess, Schlenker, Bonfait, Marcus *et al.*, 1997; Hess, Schlenker, Bonfait, Ohm *et al.*, 1997).

This series of quasi-two-dimensional monophosphate tungsten bronzes is of special interest because the average conduction electron density per W atom can be varied with the *m*

parameter, although the number of 5*d*-electrons per unit cell is independent of *m* and is always 4 (Greenblatt, 1996). In this respect, this family provides a model system of quasi-two-dimensional conductors in which the physical characteristics can be studied with respect to the *m* parameter, which is directly correlated to the thickness of the conducting layers and hence the dimensionality.

A complicated structural phase diagram has been evaluated, as a function of temperature, for different MPTBp *m* values up to $m = 14$ (Foury, Pouget, Teweldemedhin, Wang, Greenblatt & Groult, 1993; Ottolenghi & Pouget, 1996). Several phase transitions at different critical temperatures T_c are observed, related to modulation wavevectors in commensurate or incommensurate relationships with the reciprocal lattice vectors. These structural transitions, associated with periodic lattice distortions, are correlated with anomalies of the electronic properties in their thermal dependence. The characteristics observed in the metallic conductivity and in the magnetic susceptibility (Schlenker, Hess *et al.*, 1996) are often well correlated to the X-ray experiments and related to a mobility change of the charge carriers and to a decrease of the density of state at the Fermi level.

The particular feature underlined by diffuse lines observed in the X-ray patterns is the evidence of two directions of the reciprocal lattice parallel to $\mathbf{a}^* + \mathbf{b}^*$ and $\mathbf{a}^* - \mathbf{b}^*$ (Foury, Pouget, Teweldemedhin, Wang, Greenblatt & Groult *et al.*, 1993). Such diagrams are achieved using the so-called 'fixed-crystal, fixed-film' method and a monochromated X-ray beam, Mo $K\alpha$ wavelength being used to study the temperature dependence of the diffuse scattering at room temperature and above, and Cu $K\alpha$ below room temperature down to 30 K (Foury *et al.*, 1991*b*). Two sets of quite intense and broad diffuse lines are observed with the general orientation $2\mathbf{a}^* + 3\mathbf{b}^*$. They are in fact composed of a juxtaposition of diffuse segments, owing to the intersection of diffuse sheets parallel to $(110)^\star$ and $(1\bar{1}0)^\star$ with the Ewald sphere. These diffuse segments are the images of quasi-one-dimensional fluctuations along the $\mathbf{a} + \mathbf{b}$ and $\mathbf{a} - \mathbf{b}$ directions of the lattice. These features are well observed for all compounds with $m \leq 8$. For $m \geq 9$, the anisotropy of the pre-transitional fluctuations can hardly be detected probably because it is blocked by a strong additional anisotropic diffuse scattering which occurs above room temperature. In addition, another set of diffuse lines perpendicular to $\mathbf{a}^*$, but observed only for some *m* values ($m = 4, 5, 6, 8$), is due to pre-transitional fluctuations along **a** (Foury, Pouget, Teweldemedhin, Wang, Greenblatt & Groult, 1993).

The three directions of the lattice, underlined by the observation of diffusion lines, $\mathbf{a}$, $\mathbf{a} + \mathbf{b}$ and $\mathbf{a} - \mathbf{b}$, can be located in a crystal structure model. They correspond to infinite chains of WO_6 octahedra sharing corners all situated parallel to the mean plane (**ab**) of a WO_3-type slab. These chains, arranged in a zigzag or staircase manner, building a sort of ribbon (Canadell *et al.*, 1990; Canadell & Whangbo, 1991*a*), are in fact located in the three basic planes $(\mathbf{a}_p,\mathbf{b}_p)$, $(\mathbf{b}_p,\mathbf{c}_p)$, $(\mathbf{c}_p,\mathbf{a}_p)$ of the perovskite reference axes. The $(\mathbf{a}_p, \mathbf{b}_p)$ plane, easily seen in Fig. 18, is normal to the projection plane; the other two are oriented symmetrically at 45° to the projection plane. These conducting chains can be regarded as the atomic material support of the instabilities. It should be noted that the two directions $\mathbf{a} + \mathbf{b}$ and $\mathbf{a} - \mathbf{b}$ are symmetrically equivalent in the orthorhombic lattices for even *m* ($m = 2, 4, 6, 8$), but also for odd *m* values ($m = 5, 7$) since the symmetry plane of their monoclinic lattice is the **ac** plane.

Diffuse lines, already observed at room temperature for $m \leq 8$, condense on cooling, first into broad diffuse spots and then into satellite reflections at a transition temperature T_c. Another set of satellite reflections can appear at lower temperatures, however, not systematically at the position of the high-temperature diffuse lines. Several successive phase transitions at different temperatures have been found in this way, two for $m = 4$, three for $m = 6$ and two for $m = 7$ with numerous harmonics. For low *m* values ($m = 4, 5, 6$), the CDW modulation has been found to be sinusoidal and long-range order occurs. For $m = 8$, incommensurate CDW transitions appear at $T_c = 220$ and 200 K, but with the establishment of short-range ordering, this lack of long-range ordering persists down to 35 K, the lowest measurement temperature. For $m \geq 9$, structural phase transitions appear above room temperature. There is only one exception ($m = 13$), for which an additional phase transition is observed at 160 K.

Data are now well known for all *m* values ranging from 4 to 14 (Foury & Pouget, 1993; Ottolenghi & Pouget, 1996). Critical temperatures T_c are obtained from resistivity measurements and structural studies (Fig. 39). Three main types of transitions have been distinguished (Schlenker, Hess *et al.*, 1996): T_{co}, observed only for high *m* values ($m \geq 9$), correspond to a commensurate distortion with doubling of the *a* parameter. However, the phenomenon is not clearly noted for $m = 10$ and $m = 11$. T_{c1} is observed for nearly all *m* values and increases rapidly with *m* up to $m = 13$, since for $m = 14$, only T_{co} is noticed. T_{c2} is only visible for low *m* values ($m \leq 8$). This second transition temperature, practically constant for $m = 4$,

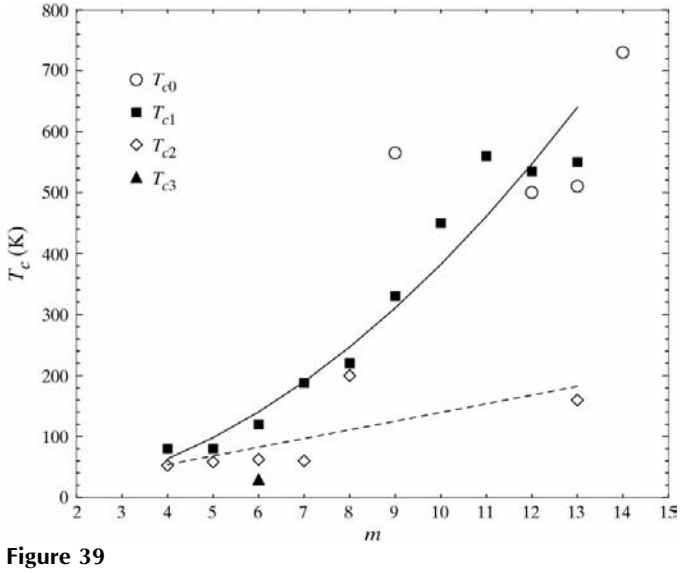

Figure 39
Critical temperatures as a function of *m*. The lines are visual guides for the T_{c1} and T_{c2} transitions.

5, 6 and 7, is lower than T_{c1} and both correspond in this domain to Peierls-type transitions. In addition, one can notice the third low-temperature transition (T_{c3}) for $m = 6$.

Another interesting diagram is the complex one giving critical wavevectors $\mathbf{q}^*$ of the different m members in the family of MPTBp (Fig. 12 of Ottolenghi & Pouget, 1996). For low m values we again find the dominant role of the **a** and **a** $\pm$ **b** chains, with the related $\mathbf{q}_a^*$ vector which slightly decreases for increasing m. Details are given in the referenced paper. Two main remarks concern the high m values. For m = 10 and 11, satellites of first order are clearly visible at room temperature with a strong intensity both at the same position: 0.43$\mathbf{a}^*$. Satellites of second order are also visible. For m = 9, 12, 13 and 14, a doubling of the cell along **a** is reported, but the modulation wavevector ($\mathbf{q}_0^*$) takes the component values (1/2 0 0) for odd m (m = 9, 13) and (1/2 0 1/2) for even m (m = 12, 14) with related satellites comparatively intense and not characteristic of a CDW. It is possible that we find here a phenomenon corresponding to the symmetry discrimination already analyzed for even and odd m values and that the structural reason for this particular modulation is due to an antiferroelectric-type distortion.

Accurate work has been performed on the analysis of the intensity along X-ray diffuse streaks and of the satellite reflections in their temperature dependence. A typical example is given in Fig. 10 of Foury & Pouget (1993), where the intensity variation of the two satellites defined by $\mathbf{q}_1^*$ and $\mathbf{q}_2^*$ in $P_4W_{12}O_{44}$ (m = 6) is measured between 20 and 120 K. The transition temperatures are then clearly defined and determined. The saturation effect can be observed but it is not general and it does not occur for example, in the m = 4 compound in the temperature range investigated down to 20 K. Elsewhere, hysteresis loops have been shown upon heating and cooling a sample of $P_4W_{28}O_{92}$ (m = 14) on a satellite reflection which induces the doubling of the cell (Ottolenghi & Pouget, 1996).

Diffuse scattering measurements of the MPTBh compound $K_xP_4W_8O_{32}$, recently realised at room and low temperature for three different compositions (x = 1.05, 1.3 and 1.94; Drouard *et al.*, 1999), show only one structural transition. A commensurate modulated structure is established with $\mathbf{q}^* = \mathbf{a}^*/2$ whatever x. Consequently, the phase transition observed at low temperature does not seem to be a Peierls transition. For x = 1.94 the lack of diffuse streaks is correlated with an ordered distribution of the K ions in the hexagonal tunnel sites (Fig. 28), whereas for weaker x values, diffuse broad lines appear on the films, either normal to **b** or along $\mathbf{a}^* + \mathbf{b}^*$ and $\mathbf{a}^* - \mathbf{b}^*$ as in MPTBp's.

4.1.2. Fermi surface nesting mechanism. The concept of hidden one-dimensional nesting of the Fermi Surface (FS) has been introduced to justify the occurrence of the CDW's in such oxides (Whangbo *et al.*, 1991; Canadell & Whangbo, 1991*b*). A Peierls transition is due to a coupling between a particular phonon and the conduction electron states. In weak coupling cases, the existence of a CDW is due to the high degree of nesting of the FS for the $\mathbf{q}^*$ critical wavevector. Above T_c, the observation of one-dimensional pretransitional fluctuations in MPTBp's, which however clearly exhibits two-dimensional electronic properties, strongly suggests that the CDW instability could arise from the quasi-one-dimensional character of the electronic structure parallel to atomic chain directions in the structure. The chain directions evidenced along **a**, **a** + **b** and **a** − **b** give rise to large flat portions of the FS which comprise bands of different orientations and which were obtained by tight-binding band calculations neglecting interslab coupling (Canadell & Whangbo, 1991*a*). The orientation and position with respect to Bragg reflections of the X-ray diffuse lines are measured from the patterns and the Fermi vectors $k_F(\mathbf{a} \pm \mathbf{b})$ and $k_F(\mathbf{a})$ of each quasi-one-dimensional portion of the FS may be deduced; they can also be calculated (Canadell & Whangbo, 1990, 1991*a*, 1993; Canadell *et al.*, 1990). These vectors are not independent and the electron conservation law leads to a relationship between their magnitudes expressed in reciprocal units: $4k_F(\mathbf{a} \pm \mathbf{b}) + 2k_F(\mathbf{a}) = 1$, which is roughly fulfilled for the m = 4, 5 and 6 members (Roussel, Foury *et al.*, 1999; Beierlein *et al.*, 1999; Foury & Pouget, 1993), although the FS evolves continuously from m = 4 to m = 6. Elsewhere, a critical wavevector may be selected so that a single modulation can simultaneously nest two differently oriented FS. In other words, the wavevector, which is stabilized, connects the cross points of sets of one-dimensional FS taken pairwise. It is expected that such a mechanism leads to an energy gain on the two differently oriented FS.

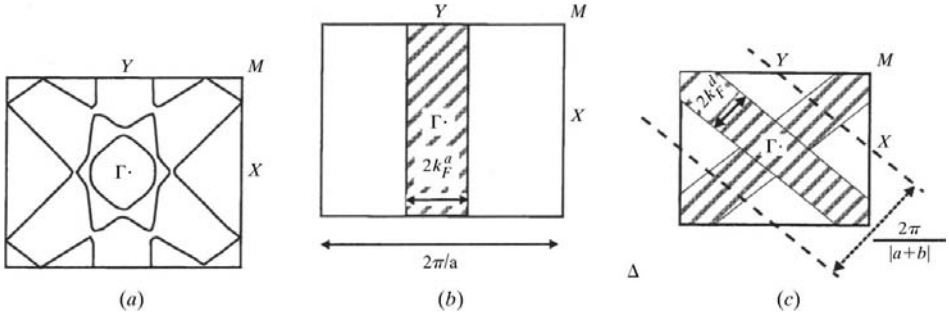

Figure 40
(*a*) Combined Fermi Surface (FS) of $P_4W_{12}O_{44}$, and its decomposition into (*b*) a one-dimensional FS associated with the chains running along **a**, and (*c*) two one-dimensional FS associated with the chains running along **a**±**b**.

The hidden nesting mechanism, by which several quasi-one-dimensional parts of the FS are connected *via* a unique modulation vector, may be realised in several ways, as can be seen for $P_4W_{12}O_{44}$. The band structure of $P_4W_{12}O_{44}$ (m = 6) has been published (Wang *et al.*, 1989*b*; Wang, Greenblatt, Rachidi, Canadell, Whangbo & Vadlamannati, 1989*b*) and has been presumed to be similar for the other members of the series (Fig. 40). Schematically, this band structure may be seen as

composed of three one-dimensional FS perpendicular to the quoted chain directions **a**, **a** + **b** and **a** − **b**. The $\mathbf{q}_1^*$ first modulation vector, stabilized at 120 K, has been chosen (Foury & Pouget, 1993) to realise simultaneously the nesting of the two oblique sets of the warped FS (Fig. 41). However, as $\mathbf{q}_1^*$ nesting is not perfect, pockets of holes are formed about the Γ point and, correlatively, pockets of electrons remain around the *M* point. Pockets of opposite carriers may be linked by $\mathbf{q}_2^*$, the modulation vector of the second modulation at 62 K. However, experiments also show that $\mathbf{q}_2^*$ defines satellites located on diffuse lines associated with the **a** chains, suggesting that such modulation could be equally stabilized by a common nesting with the one-dimensional FS of these chains.

Physical properties of $K_xP_4W_8O_{32}$ were studied for $0.75 \leq x \leq 2$ (resistivity, magnetoresistance, Hall effect and specific heat; Drouard *et al.*, 2000; Roussel *et al.*, 1997). The transition temperatures measured from the resistivity curves show a maximum $T_c \simeq 170$ K for $x = 1.3$ attributed to a maximum density of states. Note that, recently, interesting results were obtained using photoemission experiments for MPTBp's, $4 \leq m \leq 12$ (Witkowski *et al.*, 1997; Guyot *et al.*, 2000). The Fermi surface image, obtained by angle-resolved UV photoemission performed on $P_4W_8O_{32}$, shows quasi-one-dimensional bands characteristic of the hidden nesting properties, in agreement with the band structure calculations.

4.2. Modulated structures

Only two modulated structures in the MPTBp's have been studied in detail and allow a better understanding of the structural origins of the CDW: $P_4W_{20}O_{68}$ ($m = 10$) (Roussel, Labbé, Leligny *et al.*, 2000) and $P_4W_8O_{32}$ ($m = 4$; Ludecke *et al.*, 2000). The first one ($m = 10$) exhibits satellite reflections at room temperature with a strong intensity; nevertheless, crystals are always twinned with splitting of the reflections and, as the WO_3-type slabs are of large thickness, numerous defects can be included in the samples, and crystals have been found to be of poor quality. This disadvantage does not occur in the second one ($m = 4$), for which the quality appears to be extremely good, but satellite reflections are weak and they only occur at low temperatures.

4.2.1. $P_4W_{20}O_{68}$ ($m = 10$). Intense satellite reflections of first and second order were observed; third-order satellite reflections are not visible using a CAD-4 diffractometer with a classical X-ray generator. Reflections are systematically split, showing a twin with a monoclinic distortion from the orthorhombic basic lattice, the γ angle being slightly different from 90°. The $\mathbf{q}^* = 0.43\mathbf{a}^*$ modulation vector was refined by least-squares using the positions of 15 first-order satellite reflections. It should be noticed that the high-temperature pretransitional structural fluctuation of $P_4W_{20}O_{68}$ ($m = 10$) appears in the form of a broad diffuse segment centred at $0.5\mathbf{a}^*$ and extending along the $\mathbf{c}^*$ direction. On cooling from ∼600 K, the diffuse scattering sharpens and the wavevector $\mathbf{q}_d^*$ decreases from $0.5\mathbf{a}^*$ to lock at ∼400 K to the value $0.43\mathbf{a}^*$, which is observed at room temperature (Ottolenghi & Pouget, 1996). This fact, also observed for $m = 11$, reveals an unusual behaviour in this series of oxides.

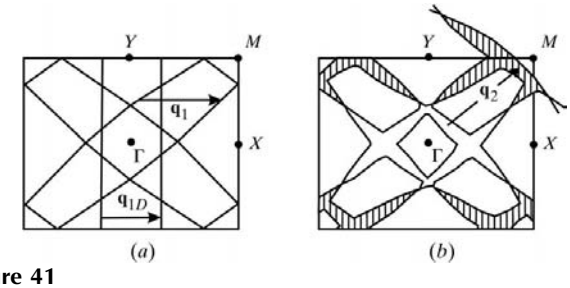

Figure 41
(*a*) Schematic FS of $P_4W_{12}O_{44}$. The $\mathbf{q}_1^*$ wavevector observed below T_{c1} is indicated. (*b*) Schematic representation of the electron-hole pockets in the oblique sheets of the FS formed by the $\mathbf{q}_1^*$ modulation and location of their hybridization wavevector $\mathbf{q}_2^*$.

The component along $\mathbf{a}^*$ is very close to 3/7, the corresponding modulation was considered as commensurate with a superstructure of period 7**a**. However, to reduce the correlation between the different refinement parameters, the four-dimensional formalism [de Wolff *et al.*, 1981; superspace group: $P2_1(\alpha 00)0$] is more suitable than a classical approach based on the supercell (7**a**, **b**, **c**) and was used to determine a model for the displacive modulation of $P_4W_{20}O_{68}$ (Roussel, Labbé, Leligny *et al.*, 2000). As expected from the strong intensity of the satellites, refinements showed that the W atoms undergo a significant displacement modulation, whereas O and P seem not to be significantly affected. In other words, the polyhedral structure is not disturbed through the modulation effects. Hence, the tilting of quite regular WO_6 octahedra and PO_4 tetrahedra is maintained, similar to that observed in the high-temperature form of all the *m* members.

The best way to visualize the W displacement inside the different WO_6 octahedra is to consider a 'segment' of 10 octahedra sharing corners which run obliquely across a WO_3-type slab. The most important result of the refinement of the modulated structure of $P_4W_{20}O_{68}$ is that the ten independent W atoms of the same segment are all displaced with respect to their position in the average structure. These displacements are approximately parallel to the direction of the segment and all displacements in one segment are pointing in the same direction. Fig. 42 shows an oblique section of a slab, one octahedron thick, showing several such segments of ten WO_6 octahedra. The selected segments include displacements among the longest, the maximum being 0.19 Å.

The two segments located on each side of the highlighted segment (Fig. 42) involve W displacements oriented in the opposite direction with respect to this segment, suggesting an antiferroelectric (AFE)-like order. The modulation which involves $\mathbf{q}_0^* = 1/2\mathbf{a}^*$ as the wavevector ($m = 9$, 12, 13 14) could be perceived as an alternate change of W displacements, regularly reversed along **a** in every other segment. Here, however, $\mathbf{q}_d^* = 3/7\mathbf{a}^*$ disturbs this regularity. The observed sequence along **a** should introduce faults, either a weak or negligible W displacement, or two consecutive displacements in the same direction in order to ensure the 7**a** periodicity. This fact suggests that if the W displacements conferred a ferroelectric polarization to a segment, it could be no real compensation for the whole set of segments in a slab. As the structure is polar, the compound could be ferroelectric, with a

polarization along **c**. Note, however, that all along a given segment, the W displacement, sometimes weak, can occur in opposite directions, leading to a more complex structural model.

In fact, all four segments located around the highlighted segment involve displacements mainly oriented in the opposite direction (in addition to the two drawn in Fig. 42, two others can be obtained from a translation **a** ± **b**). Such an arrangement is reminiscent of the low-temperature ε-form of tungsten trioxide WO_3, in which the presence of ferroelectricity is known (Woodward *et al.*, 1997). Indeed, an inequality of W shifts in a direction labelled z has been observed, which induces a net spontaneous polarization along the **c** axis of the ε-phase of WO_3.

Thus, as already pointed out, if no structural tilt model is found among the numerous antiferrodistortive transitions of WO_3 related to the different kinds of rotations of the WO_6 octahedra, then there is some resemblance with the W displacements of the low-temperature form. This viewpoint reinforces the assumption that, for large values of m, the structure of the slab tends to that of WO_3, in spite of the influence of the PO_4 tetrahedra on each side.

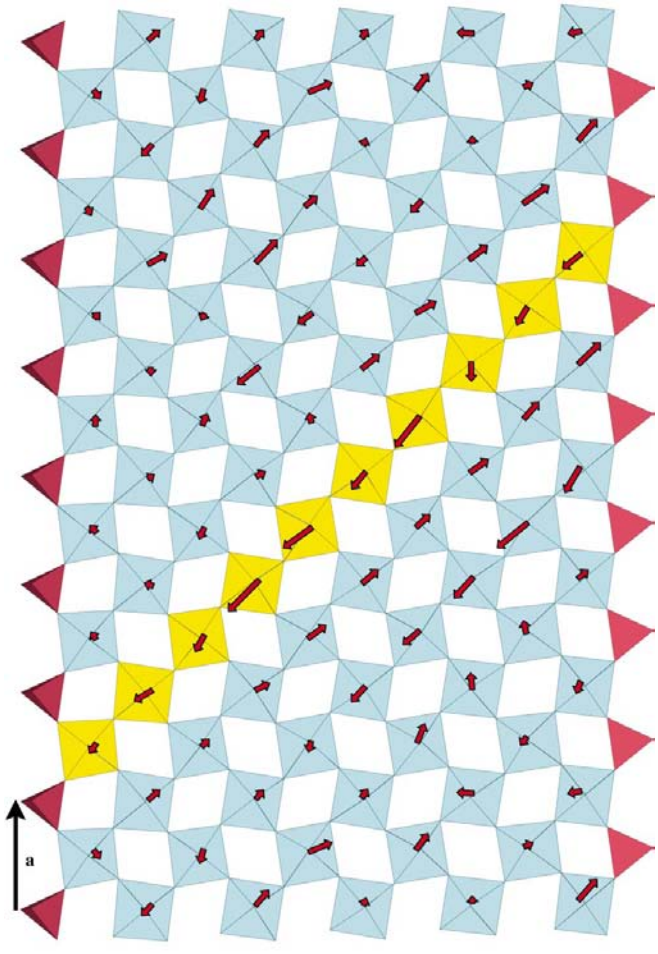

Figure 42
Section of one WO_3 layer of the **7a** × **b** × **c** supercell of $P_4W_{20}O_{68}$ with a plane defined by the **a** direction and the [12 8 1] direction of the segment of ten WO_6 octahedra outlined in Fig. 41. The arrows represent, magnified by 10, the W displacements with respect to their position in the average structure.

The ferroelectric-like displacements of the W atoms all along a segment from their average position in their octahedra, and the AFE-like order between neighbouring segments, imply a change of the interatomic distances which induces a modulation of the electron density. The formation of a CDW is thus achieved through a first-order electron-phonon coupling. A similar mechanism is required to achieve the simultaneous nesting of the differently oriented one-dimensional Fermi surfaces previously mentioned.

Another interesting structural aspect involving the W displacement is that the two directions **a** + **b** and **a** − **b**, that were equivalent in the orthorhombic lattice, are no longer symmetrical in the monoclinic lattice (γ = 90.60°). The W displacements generate the monoclinic distortion which induces the existence of two twin components, since two different directions of segments including ten WO_6 octahedra may be involved. Note that the same monoclinic distortion is observed for the m = 12, 13 and 14 members of the series and for m = 10, upon heating, the symmetry becomes effectively orthorhombic above T_c = 450 K.

4.2.2. $P_4W_8O_{32}$ (m = 4). The structural study of the modulation of $P_4W_8O_{32}$ (m = 4) required low-temperature measurements. Two phase transitions were reported to occur at T_{c1} = 80 K and T_{c2} = 52 K for the first and second CDW, respectively (Foury & Pouget, 1993). The diffuse scattering condenses into satellite reflections of weak intensity compared with those of the Bragg lattice reflections in the high-temperature form. Thus, below T_{c1} the wavevector $\mathbf{q}_1^* = 0.330\mathbf{a}^* + 0.295\mathbf{b}^*$ occurs and below T_{c2} both $\mathbf{q}_1^*$ and $\mathbf{q}_2^* = 0.340\mathbf{a}^*$ are observed.

The previous results can be elucidated in two different ways. First, the actual symmetry of both low-temperature forms remains orthorhombic as with the room-temperature form ($P2_12_12_1$) and hence $P_4W_8O_{32}$ undergoes a two-dimensional modulated structure below T_{c1} (80 K) as well as below T_{c2} (52 K). The two vectors $\mathbf{q}_1^*$ and $\mathbf{q}_1'^*$, symmetric to $\mathbf{q}_1^*$ with respect to (100)*, are then related by orthorhombic symmetry. They allow the definition of all the first-order satellite reflections. The mixed second-order satellite reflections can be described by $\mathbf{q}_2^*$ such as $\mathbf{q}_1^* - \mathbf{q}_1'^* = 1 - \mathbf{q}_2^\star$ by a numerical coincidence (Ludecke *et al.*, 2000) and there is no more symmetry breaking at T_{c2}. Secondly, the actual symmetry of both low-temperature forms becomes monoclinic and then, $\mathbf{q}_1^*$ and $\mathbf{q}_2^*$ are independent. In this case, $P_4W_8O_{32}$ would present a one-dimensional modulated structure ($\mathbf{q}_1^*$) for $T_{c2} < T < T_{c1}$ superimposed to another one, characterized by $\mathbf{q}_2^*$, below T_{c2}.

The first hypothesis is very attractive owing to its obvious simplicity. Nevertheless, two independent phase transitions have been observed (Schlenker, Hess *et al.*, 1996; Foury & Pouget, 1993). However, in the orthorhombic interpretation the existence of the satellite reflections observed below T_{c2} should no longer be induced by a symmetry-breaking phase transition, but rather by a continuous magnification of the amplitude of the modulation observed below T_{c1}. The mono-

clinic hypothesis can help us to understand the existence of two independent successive phase transitions at T_{c1} = 80 and T_{c2} = 52 K.

Let us now consider the analogous case of the m = 6 compound. $P_4W_{12}O_{44}$ exhibits two phase transitions at T_{c1} = 120 K and T_{c2} = 62 K. The wavevectors $\mathbf{q}_1^* = 0.385\mathbf{a}^*$ and $\mathbf{q}_2^* = 0.310\mathbf{a}^* + 0.295\mathbf{b}^*$ are respectively associated with these transitions (Schlenker, Hess *et al.*, 1996; Foury & Pouget, 1993). Between the m = 4 and m = 6 compounds, the primary and the secondary modulations, as defined in the first hypothesis for the m = 4 phase, have interchanged their stability range. If the orthorhombic symmetry is maintained at low temperature, only the $\mathbf{q}_2^*$ and $\mathbf{q}_2'^*$ wavevectors allow a description of the whole diffraction pattern, since $1 - \mathbf{q}_1^* = \mathbf{q}_2^* - \mathbf{q}_2'^*$, where $\mathbf{q}_2'^*$ is symmetric to $\mathbf{q}_2^*$ with respect to $(100)^*$. In such an interpretation, $\mathbf{q}_1^*$ mixed second-order satellite reflections are observed in a temperature range (between 62 and 120 K), where the first-order satellite reflections, related to $\mathbf{q}_2^*$, do not exist or have a much weaker intensity than the first-order satellite reflections. For $P_4W_{12}O_{44}$ the monoclinic hypothesis, which eliminates this problem uniquely, seems to be more appropriate.

$P_4W_8O_{32}$ and $P_4W_{12}O_{44}$ have very similar structures at room temperature and thus it is not realistic to consider two different descriptions to explain their modulated structure. In addition, the physical properties of these two compounds are very similar in their modulated phases.

Considering the even m members of the MPTBp's, all of them exhibit orthorhombic symmetry in their high-temperature phases (HT), but the high values of m, for which the low-temperature phases (LT) were stabilized, present a weak monoclinic distortion increasing with m (Table 1: $\gamma = 91.04^\circ$ for m = 14, $\gamma = 90.72^\circ$ for m = 12 and $\gamma = 90.60^\circ$ for m = 10). A still weaker distortion can then be expected for the m = 4 and m = 6 members. Note that, owing to the existence of systematic twins, as shown especially in $P_4W_{20}O_{68}$, such a weak distortion is not easy to observe. Moreover, twins permit the generation of satellite reflections corresponding to the existence of the $\mathbf{q}_1'^*$-like wavevector through the $(100)^*$ twin plane, giving an aspect of the orthorhombic symmetry to the diffraction pattern.

All these remarks underline the possibility of a monoclinic distortion both for $P_4W_8O_{32}$ and for $P_4W_{12}O_{44}$ at low temperature. Studies of these two compounds, in the monoclinic symmetry hypothesis, must be performed at $T_{c2} < T < T_{c1}$ and at $T < T_{c2}$ to clarify this point.

The present structure has been solved as an orthorhombic two-dimensional (with two symmetry-related wavevectors) incommensurate modulated structure [superspace group $P2_12_12_1(\alpha, \beta, 0)$] using synchrotron data collected at 20 K ($< T_{c2}$; Ludecke *et al.*, 2000). Importantly, the major modulation amplitudes were found, as for the structure of $P_4W_{20}O_{68}$ (m = 10), to act on the two independent W atoms and apparently not on the P and O atoms. The amplitude of the W displacements are clearly weaker for m = 4 than for m = 10 (maximum 0.070 Å, compared with 0.19 Å for m = 10) and different for the two independent W atoms. Structural sections analogous to those realised for the m = 10 compound do not reveal particular systematics for the overall W displacements (Figs. 43 and 44). However, it can be observed that all the components of these displacements normal to **a** remain weak (Fig. 43). There is no particular W displacement along the direction of a segment of four WO_6 octahedra. Rather, the strongest W displacement is oriented towards an edge of the WO_6 octahedra.

5. Diphosphate tungsten bronzes with hexagonal tunnels (DPTBh)

5.1. Lattices and symmetries

Historically this is the first family of phosphate tungsten bronzes which was discovered. To date, however, few measurements of physical properties have been performed and little crystallographic data has been collected. Results from X-ray powder or single-crystal diffraction, and electron microscopy investigations are summarized in Table 3.

The members of this series of oxides with the general formula $A_x(P_2O_4)_2(WO_3)_{2m}$ crystallize with a structural principle previously described in §2.3.1. Regular slabs of ReO_3-type, whose thickness is determined by the m parameter, are

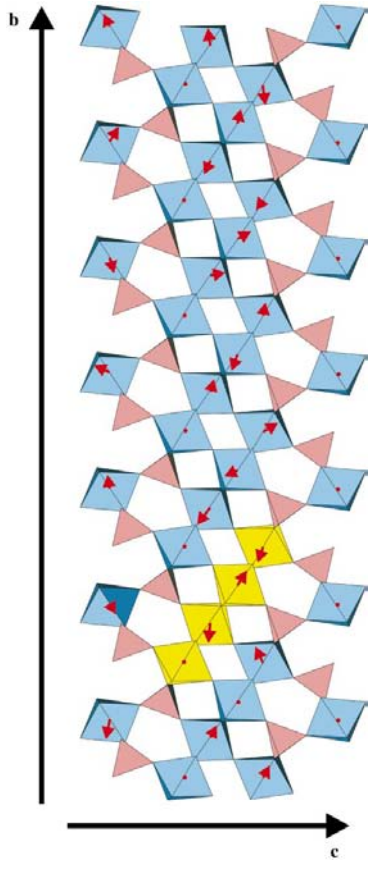

Figure 43
Projection along [100] of the average structure of $P_4W_8O_{32}$. A segment of four octahedra is highlighted. The arrows represent, magnified by 50, the W displacements with respect to their position in the average structure.

Table 3
The DPTBh series.

m	Formula	*a* (Å)	*b* (Å)	*c* (Å)	β (°)	Space group	References
4	$RbP_4W_8O_{32}$	10.181 (6)	7.519 (1)	17.156 (4)	113.32 (3)	*A*2/*m*	(*a*) (*b*)
5	$KP_4W_{10}O_{38}$	11.061	7.500	17.133	93.78		(*b*)
	$RbP_4W_{10}O_{38}$	11.091	7.522	17.140	93.78		(*b*)
6	$KP_4W_{12}O_{44}$	14.006	7.530	17.056	114.30	*A*2/*m*	(*b*), (*c*)
	$RbP_4W_{12}O_{44}$	13.991 (3)	7.530 (1)	17.122 (2)	114.22 (1)	*A*2/*m*	(*d*)
	$BaP_4W_{12}O_{44}$	14.103 (3)	7.494 (1)	17.027 (5)	114.19 (2)	*A*2/*m*	(*e*)
7	$KP_4W_{14}O_{50}$	14.618	7.508	17.098	98.99	$P2_1/c$	(*b*), (*c*)
	$RbP_4W_{14}O_{50}$	14.638	7.534	17.070	99.00	$P2_1/c$	(*b*)
	$RbP_4W_{14}O_{50}$	15.723 (4)	7.528 (6)	17.118 (4)	113.42 (2)	$P2_1/c$	(*f*)
	$BaP_4W_{14}O_{50}$	14.713 (3)	7.487 (2)	17.175 (7)	99.41 (3)	*A*2/*m*	(*e*)
8	$KP_4W_{16}O_{56}$	16.208 (8)	7.540 (4)	17.087 (8)	93.92 (4)	$P2_1/c$	(*g*)
	$RbP_4W_{16}O_{56}$	16.209 (11)	7.547 (3)	17.095 (7)	93.99 (4)	$P2_1/c$	(*g*)
	$RbP_4W_{16}O_{56}$	16.194 (3)	7.5438 (8)	17.095 (4)	93.82 (2)	$P2_1/c$	(*h*)
	$BaP_4W_{16}O_{56}$	17.910 (2)	7.480 (2)	17.0606 (9)	114.74 (1)	*A*2/*m*	(*i*)
	$BaP_4W_{16}O_{56}$	18.271 (4)	7.491 (2)	17.346 (4)	117.46 (2)	*A*2/*m*	(*e*)
	$TlP_4W_{16}O_{56}$	16.208 (8)	7.540 (4)	17.087 (8)	93.92 (4)	$P2_1/c$	(*g*)
9	$KP_4W_{18}O_{62}$	18.143	7.532	17.120	101.54	$P2_1/c$	(*b*)
	$RbP_4W_{18}O_{62}$	18.069	7.556	17.163	102.53	$P2_1/c$	(*b*)
10	$KP_4W_{20}O_{68}$	21.386	7.534	16.968	113.57	$P2_1/c$	(*b*)
	$KP_4W_{20}O_{68}$	19.589 (3)	7.5362 (4)	16.970 (3)	91.864 (14)	$P2_1/c$	(*j*)
	$RbP_4W_{20}O_{68}$	21.395	7.552	17.063	113.93	$P2_1/c$	(*b*)
	$BaP_4W_{20}O_{68}$	23.193 (4)	7.487 (2)	17.175 (7)	99.41 (3)	*A*2/*m*	(e)

References: (*a*) Giroult *et al.* (1983); (*b*) Hervieu & Raveau (1982); (*c*) Wang, Greenblatt, Rachidi, Canadell & Whangbo (1989*b*); (*d*) Giroult *et al.* (1981*b*); (*e*) Domengès, Hervieu & Raveau (1984); (*f*) Giroult *et al.* (1982*b*); (*g*) Giroult *et al.* (1981*a*); (*h*) Giroult *et al.* (1980); (*i*) Lamire *et al.* (1987*b*); (*j*) Labbé *et al.* (1983).

connected through P_2O_7 diphosphate units which, with the WO_6 octahedra, form large tunnels of hexagonal section in which the *A* cations are inserted. The cation sites, situated at the centre of the tunnels (Fig. 8), are always partially occupied ($\leq 50\%$). Only, large cations ($r_{cation} > 1.33$ Å, *e.g.* K, Rb, Tl, Ba) are localized in the hexagonal tunnels.

The *c* parameter of the monoclinic lattice is always ~17 Å. Owing to the position of the P_2O_7 groups at different *y* levels, two neighbouring hexagonal tunnels are not always connected by a lattice translation. The **c** vector sets up the correspondence every second tunnel only.

Superstructure reflections are often well observed in the electron micrographs; they reflect a doubling of the *b* parameter. Nevertheless, they give rise to few measurable intensities within the whole X-ray diffraction experiments. This phenomenon can have different possible origins:

(i) the periodicity of the P_2O_7 groups along **b**;

(ii) the tilting of the octahedra and the slight displacements of W atoms, which differ for two WO_6 octahedra stacked along **b**; and

(iii) the possible order of the cations distributed in the hexagonal tunnels.

Only the average structures of the DPTB's are solved; no quantitative information concerning the superstructure has been obtained. Nevertheless, the true symmetry of these compounds can be determined unambiguously thanks to the observation of both X-ray and electron diffraction patterns. Two space groups, *A*2/*m* and $P2_1/c$, dependent on the inserted cation, have been observed for the different members of the series. This point, along with the knowledge of the average structure and the HREM studies, have suggested models for the superstructure.

All the Ba compounds, whatever the *m* value ($6 \leq m \leq 10$), only crystallize in *A*2/*m*, in contrast to the alkaline metal DPTB's which exhibit the two previous space groups according to the *m* values: *A*2/*m* for *m* = 4, 5 and 6; $P2_1/c$ for *m* = 7, 8, 9 and 10 (Table 3). It can be envisaged that both symmetries lead to distinct structural models. Yet, a comparison of two rows of hexagonal tunnels in $BaP_4W_{16}O_{56}$ (*m* = 8, *A*2/*m*; Lamire *et al.*, 1987*b*) and in $Rb_xP_4W_{16}O_{56}$ (*m* = 8, $P2_1/c$; Giroult *et al.*, 1980) shows that the polyhedral arrangement is exactly the same, with a symmetry centre and/or a twofold axis in the middle of the hexagonal tunnels, delimited on each side by two P_2O_7 groups at the same *y* level, and a 2_1 axis through the rhombic tunnels (Figs. 45*a* and *b*). The reason is that $P2_1/c$ is a subgroup of *A*2/*m*. However, along a row of hexagonal tunnels, another effective possibility exists. It has been observed for $KP_4W_{20}O_{68}$ (*m* = 10; Labbé *et al.*, 1983) corresponding to a total shift (**c**/4) of all the symmetry elements with respect to the Rb compounds. The symmetry centres are thus located in the rhombic tunnels, whereas the 2_1 axes occupy all the hexagonal tunnels, delimited now on each side by P_2O_7 groups at different *y* levels (Fig. 45*c*).

However, examination of Table 3 reveals another point. For a given *m*, the published values of *a* and β are sometimes different from one compound to another, although the product $a \times \sin\beta = d_{100}$ remains constant. This phenomenon is independent of the choice of monoclinic axes. Thus, the two structural models with *m* = 8, $BaP_4W_{16}O_{56}$ and $Rb_xP_4W_{16}O_{56}$, are not rigorously superimposable (Fig. 45). In the Ba compound, the **a** translation is parallel to a linear chain of WO_6 octahedra; in the Rb compound, **a** takes a different orientation owing to a **c**/2 shift of a slab with respect to the next. The distribution of the P_2O_7 groups around the hexagonal tunnel along a row of these tunnels remains exactly the same, but the **c**/2 shift involves two different lattices. This feature shows the great adaptability of the diphosphate units to a WO_3-type structure. As in the monophosphate tungsten bronzes, the connection of two identical slabs may be achieved in different ways, because although the polyhedra remain roughly regular in general, their flexibility leads to several linkage possibilities. Moreover, several arrangements have been suggested with P_2O_7 groups at different heights on each side of the hexagonal tunnels within a single sample (Lamire *et al.*, 1987*b*).

5.2. Tilting modes of the WO_6 octahedra and W displacements

The tilting mode of the WO_6 octahedra, insofar as it can be deduced from the structural studies of DPTB's, is more difficult to understand than that found in the MPTB's. Indeed, only the average structures have been solved so that we have only the average positions of the O atoms from which to draw conclusions. It seems that the influence of the diphosphate groups in the DPTBh's is more important than in the MPTB's. For example, in Rb compounds with $m = 8$, the WO_6 octahedra located in the middle part of a slab, surrounded only by six other octahedra, are quite regular and untilted. A progressive tilted distortion is observed when the distances from the diphosphate groups decrease. The maximal tilt is observed for the octahedron linked to two tetrahedra. Each tilted octahedron is rotated about one of its medians, which joins in the (010) projection plane two opposite sides (Fig. 46*b*), whereas in monophosphates the octahedra are rotated about one of its axes. Conversely, in the $m = 10$ compound (Fig. 46*d*), where the slabs become larger and whose structure are closer to that of WO_3, the octahedra are rotated along an oblique segment crossing the slab, the ten WO_6 octahedra sharing corners being tilted in a staggered manner, and such a deformation occurs from one end to the other of the segment enclosed by the diphosphate groups. Over the complete series, two types of arrangement are observed depending on whether the configurations of the P_2O_7 groups at both ends of a segment are located at the same level or are shifted by **b**/2. Within a segment, the terminal octahedron, linked to two tetrahedra, and the next, linked to one tetrahedron, must fit their tilt to the geometry of the P_2O_7 groups (Fig. 46*a*, *b*, *c* and *d*). This fact, which is related to the relative distribution of the diphosphate groups along all of the hexagonal tunnels is, consequently, directly imposed by the tilting process.

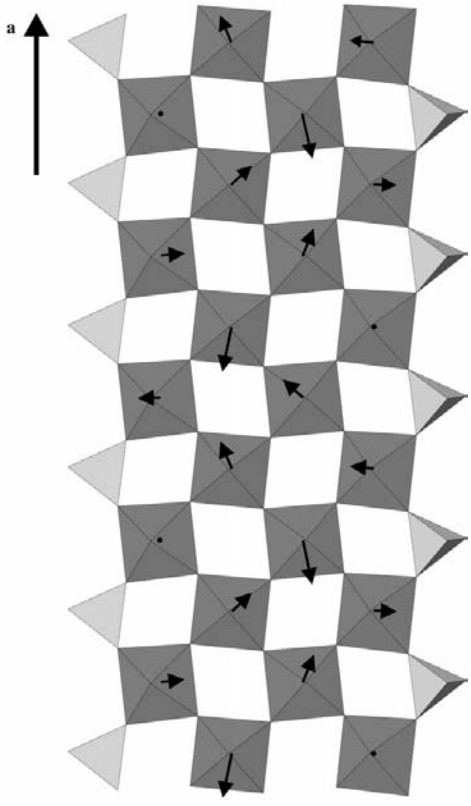

Figure 44
Section of one WO_3 layer of the $7\mathbf{a} \times \mathbf{b} \times \mathbf{c}$ supercell of $P_4W_{20}O_{68}$ with a plane defined by the **a** direction and the $[01\bar{1}]$ direction of the segment of four WO_6 octahedra outlined in Fig. 43. The arrows represent, magnified by 50, the W displacements with respect to their position in the average structure.

For all the compounds of the series, whatever their space group, the X-ray single-crystal determinations have shown that the displacement of the W atoms along **b** with respect to the (010) mean plane of these atoms is always weak. This explains the low number of superstructure reflections which give rise to observable or measurable intensities. However, the W atoms are not localized at the centre of the octahedra, always being displaced so that the W atoms located in the central part of the slabs have the most regular oxygen environment with a small dispersion of the six W—O distances. This dispersion increases regularly by moving away towards the tetrahedra (Fig. 47), and the tendency to a 3 + 3 (or 4 + 2) coordination for W is clearly observed when the number of tetrahedra linked to the octahedron increases. These features, also noted for MPTB's, can be related to the mean value of the oxidation state of the tungsten, W^V having a tendency to be satisfied by an ideal octahedral coordination and W^{VI} with a 4 + 2 coordination.

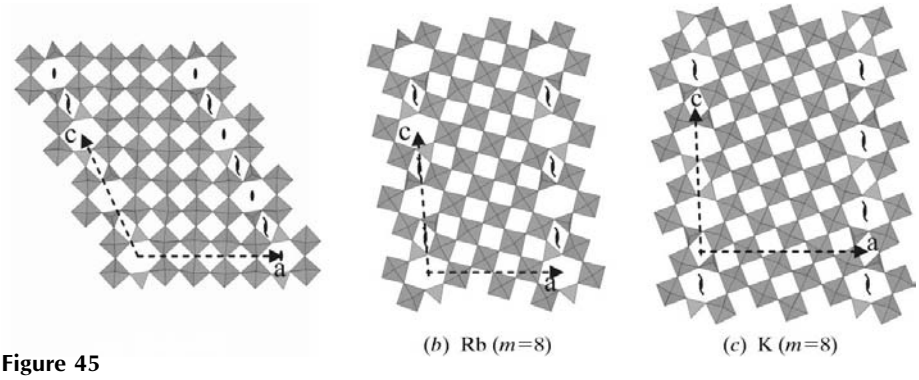

Figure 45
Distribution of the symmetry elements in (*a*) $BaP_4W_{16}O_{56}$ ($A2/m$), (*b*) $RbP_4W_{16}O_{56}$ ($P2_1/c$) and (*c*) $KP_4W_{20}O_{68}$ ($P2_1/c$).

5.3. Stacking faults and dislocations

Several HREM studies have been published on the structural relationships within DPTBh's with Rb, K and Ba as cations inserted in the hexagonal tunnels (Hervieu & Raveau, 1983*a*,*b*, 1982; Hervieu *et al.*, 1985*b*; Domengès, Hervieu & Raveau, 1984). They showed very complex non-stoichiometry. The following faults are likely to be responsible for these features.

Irregular intergrowths of different *m* members reflecting disorder are

observed for m values larger than 10. It is thus understandable that the highest m value reached for an X-ray single-crystal determination is m = 10. Yet, from time to time, for some crystallites, regular coherent arrangements of two close m values occur. Thus, a regular intergrowth of m = 8 and m = 9 Ba compounds, with a periodicity of ∼34 Å in the direction normal to the slab, has already been observed (Fig. 48). This case proves the possibility of non-integral mean m values, here m = 8.5. Nevertheless, such intergrowth has never been stabilized as a single-crystal sample.

The interruption of P_2O_7 rows in a (100) plane and their substitution by WO_6 octahedra has been shown (Fig. 49). This other type of extended defect tends to generate microdomains of various compositions.

The existence of crystallographic shear planes (CSP) in the WO_3-type slabs has been observed. They can appear as localized defects, or in an ordered way as microphases, by the formation of regular intergrowths of CSP with the diphosphate layers. Several CSP have thus been observed with different orientations according to the thickness of the slabs: 102, 103 and mixed 001/103 (Borel *et al.*, 1991; Hervieu & Raveau, 1983*a*; Hervieu *et al.*, 1985*b*), see Fig. 50. The latter type of defect could occur under electron irradiation. The wide existence range of CSP, from isolated defect to regular sequences, suggests that their mechanisms of formation are complex.

5.4. Physical properties of DPTB's

The magnetic and electron transport properties of three DPTBh bronzes with $m = 8$, $A_xP_4W_{16}O_{56}$ (A = K, Rb, Tl), have been studied as a function of temperature (Giroult, Goreaud, Labbé, Provost & Raveau, 1981) with polycrystalline samples. The magnetic susceptibility was measured from 77 to 300 K. The three compounds are characterized by a Pauli paramagnetism, which is in agreement with the electron transport measurements. The thermoelectric power and the resistivity, studied in the range 120–650 K, show a metallic behaviour for these three oxides. The conductivity, observed at room temperature, close to $10^3\ \Omega^{-1}\ cm^{-1}$ is ten times lower than that observed for the Magneli tungsten bronzes A_xWO_3 (Magnéli & Blomberg, 1951). The metallic behaviour of these oxides is attributed to W—O—W interactions in the WO_3-type slabs with a band model proposed for Na_xWO_3 by Goodenough (1973); it is built from the overlapping of the 2p oxygen orbitals and the t_{2g} tungsten orbitals. However, the P—O bonds which ensure, in the structure, the cohesion between the octahedral slabs have a covalent character and do not contribute to the conduction. The P_2O_7 groups at the boundary of the WO_3-type slabs should involve a drastic anisotropy of the electrical properties. To verify this expected behaviour, Wang and co-workers (Wang, Greenblatt, Rachidi, Canadell & Whangbo, 1989*b*) have studied the electronic properties of two oriented single crystals, $KP_4W_{12}O_{44}$ (m = 6) and $KP_4W_{14}O_{50}$ (m = 7). The electrical resistivity measurements along the three crystallographic reciprocal axes show a quasi-two-dimensional behaviour with the resistivity, along a direction perpendicular to the slabs, being one order of magnitude larger than along the other two directions, parallel to their mean planes. Elsewhere, partial substitution of K^+ by alkali metal ions such as Li^+, Na^+ or Rb^+ leads to an

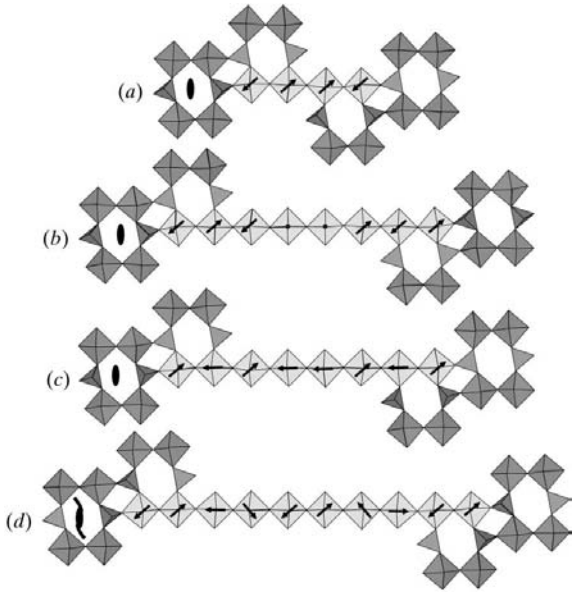

Figure 46
The octahedral chains forming the ReO_3-type slabs in the DPTBh members: (*a*) $RbP_4W_8O_{32}$; (*b*) $Rb_{0.8}P_4W_{16}O_{56}$; (*c*) $BaP_4W_{16}O_{56}$; (*d*) $KPW_{20}O_{68}$. The arrow show the tilting of the octahedra.

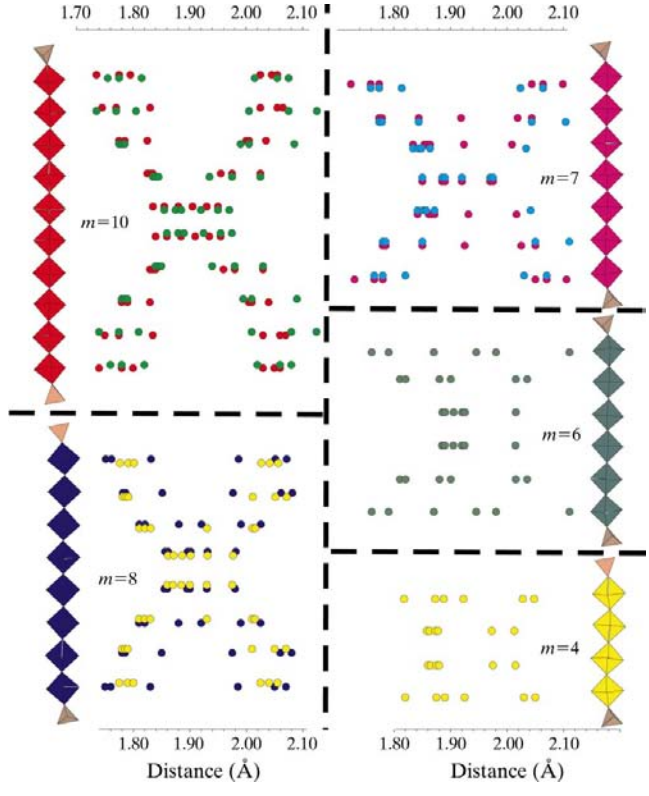

Figure 47
Dispersion of the W—O distances in the WO_6 octahedra in the DPTBh series.

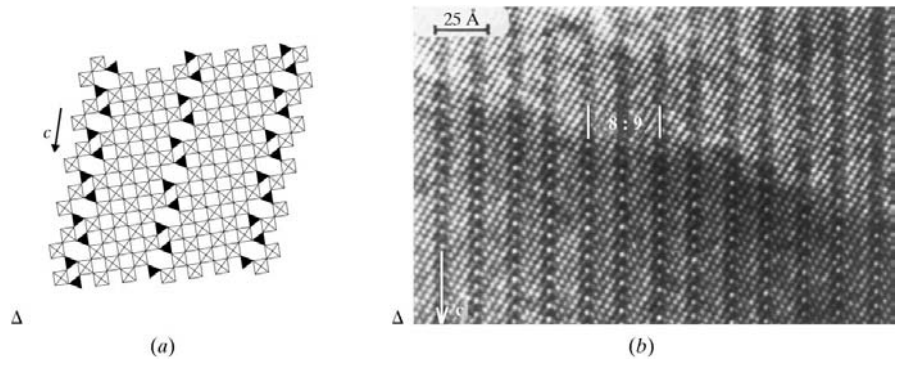

Figure 48
(*a*) Schematized structure of the regular intergrowth $2m = 8 + 9$; (*b*) HREM image: ordered intergrowth $2m = 8 + 9$ observed in the DPTBh's $A_x(P_2O_4)_2(WO_3)_{2m}$, $m = 9$ crystal.

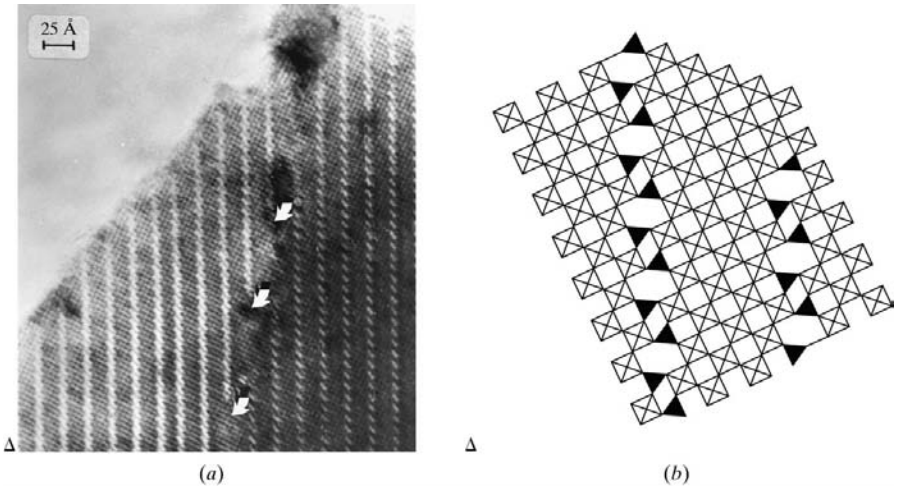

Figure 49
(*a*) Terminations of P_2O_7 rows in a $m = 11$ member, labelled a defect. (*b*) Idealized drawing of such a phenomenon.

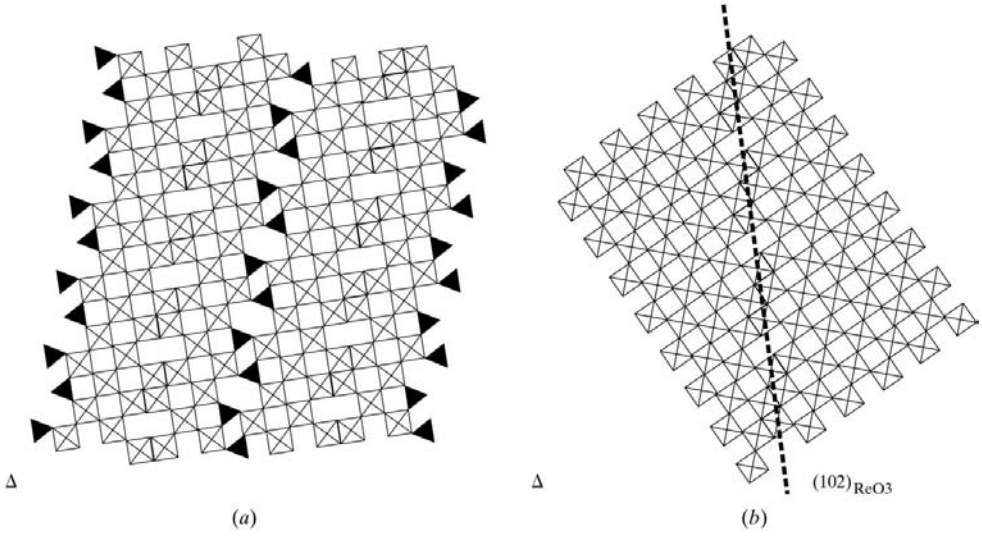

Figure 50
(*a*) Regular intergrowth of diphosphate layers with 102 CSP planes. (*b*) Intergrowth of diphosphate layers with 'combined' 103/001 CSP planes.

enhancement of the conductivity and an increase in the extent of the anisotropy.

6. Conclusions

The three main families of phosphate tungsten bronzes, MPTBp, MPTBh and DPTBh, are all characterized by specific physical behaviour. The MPTBp's exhibit the formation of successive charge density waves, different for each compound, which give rise to anomalies in the transport properties. The $\mathbf{q}^*$ wavevectors have been determined by X-ray diffuse scattering methods. The MPTBh's and DPTBh's offer other interesting features: the former exhibit, according to the ratio of cations inserted within the hexagonal tunnels, a change in the number of electrons in the partially filled electronic band, while the latter involves either mono- or two-dimensional properties according to the nature of the inserted cation. These three bronze families consequently provide an ideal tool to study the relations between band filling and electronic instabilities in a low-dimensional system.

Numerous physical and crystallographic methods have been used to obtain knowledge about these families and some other methods are currently being developed: photoemission, the use of synchrotron radiation, multidimensional formalisms for modulated structure resolution and *ab initio* calculations. All these studies are directed towards a common goal: to gather knowledge of the Fermi surface which presents a particular topology. In this context, an accurate determination of the structure, including details of the atomic modifications and subtleties in the modulated phases, is essential.

In spite of strong pseudo-symmetries and systematic twinning phenomena, mainly due to

tilting modes of the WO_6 octahedra, the structures of the MPTBp's are without doubt the best known. Nevertheless, two challenges remain to be confronted in the family $(PO_2)_4(WO_3)_{2m}$: to determine structures for the high m values ($m > 12$) and to study the modulated structure observed at room temperature as well as at low temperature.

The WO_6 tilting phenomenon induces a systematic doubling of the b lattice parameter for the diphosphate tungsten bronzes. Unfortunately, the weak intensities of the resulting superstructure reflections do not allow a solution for the actual structure of these compounds using classical X-ray diffractometers; only the average structure is available. Owing to a more complex behaviour than that of the MPTB's, the DPTBh's have been less studied from a crystallographic and physical point of view. Systematic studies of the actual structure and characterization of the transport properties of these compounds should be developed.

Authors are grateful to Dr J. P. Pouget for fruitful discussions about the 'Phase-transitions in monophosphate tungsten bronzes' section and are indebted to Professor M. Hervieu who provided us the original micrographs shown in Figs. 9, 32, 48 and 49; some of them are 20 years old. We greatly appreciate also the advice of Dr M. Korzenski.

References

Beierlein, U., Schlenker, C., Dumas, J., Groult, D., Labbé, Ph., Balthes, E. & Steep, E. (1999). *Synth. Met.* **103**, 2593–2595.

Benmoussa, A., Groult, D., Labbé, Ph. & Raveau, B. (1984). *Acta Cryst.* C**40**, 573–576.

Benmoussa, A., Groult, D. & Raveau, B. (1984). *Rev. Chim. Miner.* **21**, 710–720.

Benmoussa, A., Labbé, Ph., Groult, D. & Raveau, B. (1982). *J. Solid State Chem.* **4**, 318–325.

Borel, M. M., Goreaud, M., Grandin, A., Labbé, Ph., Leclaire, A. & Raveau, B. (1991). *Eur. J. State Inorg. Chem.* **28**, 93–129.

Brown, I. D. & Altermatt, D. (1985). *Acta Cryst.* B**41**, 244–247.

Brown, I. D. & Wu, K. K. (1976). *Acta Cryst.* B**32**, 1957–1959.

Canadell, E. & Whangbo, M. H. (1990). *J. Solid State Chem.* **86**, 131–134.

Canadell, E. & Whangbo, M. H. (1991*a*). *Phys. Rev. B*, **43**, 1894–1902.

Canadell, E. & Whangbo, M. H. (1991*b*). *Chem. Rev.* **91**, 965–1034.

Canadell, E. & Whangbo, M. H. (1993). *Int. J. Mod. Phys. B*, **7**, 4005–4043.

Canadell, E., Whangbo, M. H. & Rachidi, I. E. I. (1990). *Inorg. Chem.* **29**, 3871–3875.

Diehl, R., Brandt, G. & Salje, E. (1978). *Acta Cryst.* B**34**, 1105–1111.

Domengès, B., Goreaud, M., Labbé, Ph. & Raveau, B. (1983). *J. Solid State Chem.* **50**, 173–179.

Domengès, B., Hervieu, M. & Raveau, B. (1984). *Acta Cryst.* B**40**, 249–256.

Domengès, B., Hervieu, M. & Raveau, B. (1990). *Acta Cryst.* B**46**, 610–619.

Domengès, B., Hervieu, M., Raveau, B. & O'Keeffe, M. (1988). *J. Solid State Chem.* **72**, 155–172.

Domengès, B., Hervieu, M., Raveau, B. & Tilley, R. J. D. (1984). *J. Solid State Chem.* **54**, 10–28.

Domengès, B., McGuire, N. K. & O'Keefe, M. (1985). *J. Solid State Chem.* **56**, 94–100.

Domengès, B., Roussel, P., Labbé, Ph. & Groult, D. (1996). *J. Solid State Chem.* **127**, 302–307.

Domengès, B., Studer, F. & Raveau, B. (1983). *Mater. Res. Bull.* **18**, 669–676.

Drouard, S., Foury, P., Roussel, P., Groult, D., Dumas, J., Pouget, J. P. & Schlenker, C. (1999). *Synth. Met.* **103**, 2636–2639.

Drouard, S., Groult, D., Dumas, J., Buder, R. & Schlenker, C. (2000). *Eur. Phys. J. B*, **16**, 593–600.

Dumas, J., Beierlein, U., Drouard, S., Hess, C., Groult, D., Labbé, Ph., Roussel, P., Bonfait, G., Gomez-Marin, E. & Schlenker, C. (1999). *J. Solid State Chem.* **147**, 320–327.

Dumas, J., Hess, C., Schlenker, C., Bonfait, G., Gomez-Marin, E., Groult, D. & Marcus, J. (2000). *Eur. Phys. J. B*, **14**, 73–82.

Foury, P. & Pouget, J. P. (1993). *Int. J. Mod. Phys. B*, **7**, 3973–4003.

Foury, P., Pouget, J. P., Teweldemedhin, Z. S., Wang, E. & Greenblatt, M. (1993). *Synth. Met.* **55–57**, 2605–2610.

Foury, P., Pouget, J. P., Teweldemedhin, Z. S., Wang, E., Greenblatt, M. & Groult, D. (1993). *J. Phys. IV Fr.* **3**, 133–136.

Foury, P., Pouget, J. P., Wang, E. & Greenblatt, M. (1991*a*). *Synth. Met.* **41–43**, 3973–3974.

Foury, P., Pouget, J. P., Wang, E. & Greenblatt, M. (1991*b*). *Europhys. Lett.* **16**, 485–490.

Foury, P., Roussel, P., Groult, D. & Pouget, J. P. (1999). *Synth. Met.* **103**, 2624–2627.

Ghedira, M., Vincent, H., Marezio, M., Marcus, J. & Furcaudot, G. (1985). *J. Solid State Chem.* **56**, 66–73.

Giroult, J. P., Goreaud, M., Labbé, Ph., Provost, J. & Raveau, B. (1981). *Mater. Res. Bull.* **16**, 811–816.

Giroult, J. P., Goreaud, M., Labbé, Ph. & Raveau, B. (1980). *Acta Cryst.* B**36**, 2570–2575.

Giroult, J. P., Goreaud, M., Labbé, Ph. & Raveau, B. (1981*a*). *Acta Cryst.* B**37**, 2139–2142.

Giroult, J. P., Goreaud, M., Labbé, Ph. & Raveau, B. (1981*b*). *Acta Cryst.* B**37**, 1163–1166.

Giroult, J. P., Goreaud, M., Labbé, Ph. & Raveau, B. (1982*a*). *J. Solid State Chem.* **44**, 407–414.

Giroult, J. P., Goreaud, M., Labbé, Ph. & Raveau, B. (1982*b*). *Acta Cryst.* B**38**, 2342–2347.

Giroult, J. P., Goreaud, M., Labbé, Ph. & Raveau, B. (1983). *Rev. Chim. Miner.* **20**, 829–836.

Glazer, A. M. (1972). *Acta Cryst.* B**28**, 3384–3392.

Goodenough, J. B. (1973). *Les oxydes des métaux de transition.* Paris: Gauthier-Villars.

Greenblatt, M. (1993). *Oxide Bronzes*. Singapore: World Scientific.

Greenblatt, M. (1996). *Acc. Chem. Res.* **29**, 219–228.

Guyot, H., Motta, N., Marcus, J., Drouard, S. & Balaska, B. (2000). ECOSS 2000. Madrid, Spain.

Hervieu, M., Domengès, B. & Raveau, B. (1985*a*). *J. Solid State Chem.* **58**, 233–242.

Hervieu, M., Domengès, B. & Raveau, B. (1985*b*). *Chem. Scr.* **25**, 361–368.

Hervieu, M. & Raveau, B. (1982). *J. Solid State Chem.* **43**, 299–308.

Hervieu, M. & Raveau, B. (1983*a*). *Chem. Scr.* **22**, 117–122.

Hervieu, M. & Raveau, B. (1983*b*). *Chem. Scr.* **22**, 123–128.

Hess, C., Le Touze, C., Schlenker, C., Dumas, J. & Groult, D. (1997). *Synth. Met.* **86**, 2157–2158.

Hess, C., Le Touze, C., Schlenker, C., Dumas, J., Groult, D. & Marcus, J. (1997). *Synth. Met.* **86**, 2419–2422.

Hess, C., Schlenker, C., Bonfait, G., Marcus, J., Ohm, T., Paulsen, C., Dumas, J., Tholence, J. L., Greenblatt, M. & Almeida, M. (1997). *Physica C*, **282–287**, 955–956.

Hess, C., Schlenker, C., Bonfait, G., Ohm, T., Paulsen, C., Dumas, J., Teweldemedhin, Z. S., Greenblatt, M., Marcus, J. & Almeida, M. (1997). *Solid State Commun.* **104**, 663–668.

Hess, C., Schlenker, C., Dumas, J., Greenblatt, M. & Teweldemedhin, Z. S. (1996). *Phys. Rev. B*, **54**, 4581–4588.

Hess, C., Schlenker, C., Hodeau, J. L., Ottolenghi, A. & Pouget, J. P. (1997). *Synth. Met.* **86**, 2169–2170.

Kehl, W. L., Hay, R. G. & Wahl, D. (1952). *J. Appl. Phys.* **23**, 212–215.

Kihlborg, L. (1982). European Congress of Solid State Chemistry. Veldhoven, The Nederlands.
Kihlborg, L., Marinder, B. O., Sundberg, M., Portemer, F. & Ringaby, O. (1994). *J. Solid State Chem.* **111**, 111–117.
Kinomura, N., Hirose, M., Kumada, N., Muto, F. & Ashida, T. (1988). *J. Solid State Chem.* **77**, 156–161.
Labbé, Ph. (1992). *Diffusionless Phase Transitions and Related Structures in Oxides*, edited by C. Boulesteix. Zurich, Switzerland: Trans. Tech. Pub.
Labbé, Ph., Goreaud, M. & Raveau, B. (1978). *Acta Cryst.* B**34**, 1433–1438.
Labbé, Ph., Goreaud, M. & Raveau, B. (1986). *J. Solid State Chem.* **61**, 324–331.
Labbé, Ph., Ouachée, D., Goreaud, M. & Raveau, B. (1983). *J. Solid State Chem.* **50**, 163–172.
Lamire, M., Labbé, Ph., Goreaud, M. & Raveau, B. (1987*a*). *J. Solid State Chem.* **66**, 64–72.
Lamire, M., Labbé, Ph., Goreaud, M. & Raveau, B. (1987*b*). *J. Solid State Chem.* **71**, 342–348.
Le Touze, C., Bonfait, G., Schlenker, C., Dumas, J., Almeida, M., Greenblatt, M. & Teweldemedhin, Z. S. (1995). *J. Phys. I Fr.* **5**, 437–442.
Lehmann, J., Schlenker, C., Le Touze, C., Rötger, A., Dumas, J., Marcus, J., Teweldemedhin, Z. S. & Greenblatt, M. (1993). *J. Phys. IV Fr.* **3**, 243–246.
Loopstra, B. O. & Boldrini, P. (1966). *Acta Cryst.* **21**, 158–162.
Loopstra, B. O. & Rietveld, H. M. (1965). *Acta Cryst.* B**25**, 1420–1421.
Ludecke, J., Jobst, A., Geupel, S. & van Smaalen, S. (2001). Submitted.
Ludecke, J., Jobst, A. & van Smaalen, S. (2000). *Europhys. Lett.* **49**, 257–261.
Magnéli, A. (1948). *Acta Chem. Scand.* **2**, 861–871.
Magnéli, A. & Blomberg, B. (1951). *Acta Chem. Scand.* **5**, 372–378.
Ottolenghi, A., Foury, P., Pouget, J. P., Teweldemedhin, Z. S., Greenblatt, M., Groult, D., Marcus, J. & Schlenker, C. (1995). *Synth. Met.* **70**, 1301–1302.
Ottolenghi, A. & Pouget, J. P. (1996). *J. Phys. I Fr.* **6**, 1059–1083.
Pérez, O., Roussel, P. & Guyot, H. (2000). Two allocated days on D2B, Experiment No. 5-23-523. Technical Report. Institut Max Von Laue–Paul Langevin, Grenoble, France.
Pouget, J. P., Kagoshima, S., Schlenker, C. & Marcus, J. (1983). *J. Phys. Lett.* **44**, 113–120.
Rötger, A., Lehmann, J., Schlenker, C., Dumas, J., Marcus, J., Teweldemedhin, Z. S. & Greenblatt, M. (1994). *Europhys. Lett.* **25**, 23–29.
Rötger, A., Schlenker, C., Dumas, J., Wang, E., Teweldemedhin, Z. S. & Greenblatt, M. (1993). *Synth. Met.* **55–57**, 2670–2675.
Roussel, P., Drouard, S., Groult, D., Labbé, Ph., Dumas, J. & Schlenker, C. (1999). *J. Mater. Chem.* **9**, 973–978.
Roussel, P., Foury, P., Domengès, B., Groult, D., Labbé, Ph. & Pouget, J. P. (1999). *Eur. Phys. J. B*, **12**, 497–508.
Roussel, P., Groult, D., Hess, C., Labbé, Ph. & Schlenker, C. (1997). *J. Phys. Condensed Matter*, **9**, 7081–7088.
Roussel, P., Groult, D., Maignan, A. & Labbé, Ph. (1999). *Chem. Mater.* **11**, 2049–2056.
Roussel, P., Labbé, Ph. & Groult, D. (2000). *Acta Cryst.* B**56**, 377–391.
Roussel, P., Labbé, Ph., Groult, D., Domengès, B., Leligny, H. & Grebille, D. (1996). *J. Solid State Chem.* **122**, 281–290.
Roussel, P., Labbé, Ph., Leligny, H., Groult, D., Foury, P. & Pouget, J. P. (2000). *Phys. Rev. B*, **62**, 176–188.
Roussel, P., Masset, A. C., Domenges, B., Maignan, A., Groult, D. & Labbé, Ph. (1998). *J. Solid State Chem.* **139**, 362–372.
Roussel, P., Mather, G., Domengès, B., Groult, D. & Labbé, Ph. (1998). *Acta Cryst.* B**54**, 365–375.
Rouxel, J. (1983). *L'actualité chimique*, pp. 7–16.
Salje, E. (1977). *Acta Cryst.* B**33**, 574–577.
Sandre, E., Foury-Leylekian, P., Ravy, S. & Pouget, J. P. (2001). *Phys. Rev. Lett.* In the press.
Schlenker, C. (1989). *Low-Dimensional Electronic Properties of Molybdenum Bronzes and Oxides*, Vol. 11. Dordrecht: Kluwer Academic Publishers.
Schlenker, C., Dumas, J., Greenblatt, M. & van Smaalen, S. (1989). *Physics and Chemistry of Low-Dimensional Inorganic Conductors*, Series B: Physics, Vol. 354. Peplum Press, NATO Scientific Affairs Division: New York.
Schlenker, C., Dumas, J., Greenblatt, M. & van Smaalen, S. (1996). Physics and Chemistry of Low Dimensional Inorganic Conductors, NATO ASI Series. New York: Plenum Press.
Schlenker, C., Hess, C., Le Touze, C. & Dumas, J. (1996). *J. Phys. I Fr.* **6**, 2061–2078.
Schlenker, C., Le Touze, C., Hess, C., Rötger, A., Dumas, J., Marcus, J., Greenblatt, M., Teweldemedhin, Z. S., Ottolenghi, A., Foury, P. & Pouget, J. P. (1995). *Synth. Met.* **70**, 1263–1266.
Teweldemedhin, Z. S., Ramanujachary, K. V. & Greenblatt, M. (1991). *J. Solid State Chem.* **95**, 21–28.
Teweldemedhin, Z. S., Ramanujachary, K. V. & Greenblatt, M. (1992). *Phys. Rev. B*, **46**, 7897–7900.
Vogt, T., Woodward, M. & Hunter, B. A. (1999). *J. Solid State Chem.* **144**, 209–215.
Wang, E., Greenblatt, M., Rachidi, E. I., Canadell, E. & Whangbo, M. H. (1989*a*). *J. Solid State Chem.* **81**, 173–180.
Wang, E., Greenblatt, M., Rachidi, E. I., Canadell, E. & Whangbo, M. H. (1989*b*). *J. Solid State Chem.* **80**, 266–275.
Wang, E., Greenblatt, M., Rachidi, E. I., Canadell, E., Whangbo, M. H. & Vadlamannati, S. (1989*a*). *Phys. Rev. B*, **39**, 12969–12972.
Wang, E., Greenblatt, M., Rachidi, E. I., Canadell, E., Whangbo, M. H. & Vadlamannati, S. (1989*b*). *Phys. Rev. B*, **40**, 11964–11964.
Wang, S. L., Wang, C. C. & Lii, K. H. (1989). *J. Solid State Chem.* **82**, 298–302.
Whangbo, M. M., Canadell, E., Foury, P. & Pouget, J. P. (1991). *Sciences*, **252**, 96–98.
Witkowski, N., Garnier, M., Purdie, D., Baer, Y., Malterre, D. & Groult, D. (1997). *Solid State Commun.* **103–108**, 471–475.
Wohler, F. (1825). *Philos. Mag.* **66**, 263.
Wolff, P. M. de, Janssen, T. & Janner, A. (1981). *Acta Cryst.* A**37**, 625–636.
Woodward, P. M., Sleight, A. W. & Vogt, T. (1995). *J. Phys. Chem. Solids*, **56**, 1305–1315.
Woodward, P. M., Sleight, A. W. & Vogt, T. (1997). *J. Solid State Chem.* **131**, 9–17.
d'Yachenko, O. G., Tabachenko, V. V. & Sundberg, M. (1995). *J. Solid State Chem.* **119**, 8–12.
Yan, Y. F., Kleman, M., Le Touze, C., Marcus, J. & Schlenker, C. (1994). *13th Intl. Conf. on Electronic Microscopy*, Vol. IIB, edited by B. Jouffrey & C. Collieux, p. 909. Les Editions de Physique, Paris, 17–22 July 1994.
Yan, Y., Kleman, M., Le Touze, C., Marcus, J., Schlenker, C. & Buffat, A. (1995). *Europhys. Lett.* **30**, 49–54.